



This discussion paper is/has been under review for the journal Geoscientific Model Development (GMD). Please refer to the corresponding final paper in GMD if available.

CESM/CAM5 improvement and application: comparison and evaluation of updated CB05_GE and MOZART-4 gas-phase mechanisms and associated impacts on global air quality and climate

J. He¹, Y. Zhang¹, S. Tilmes², L. Emmons², J.-F. Lamarque², T. Glotfelty¹, A. Hodzic², and F. Vitt²

¹Department of Marine, Earth, and Atmospheric Science, North Carolina State University, Raleigh, NC, USA

²National Center for Atmospheric Research, Boulder, CO, USA

Received: 13 July 2015 – Accepted: 20 July 2015 – Published: 27 August 2015

Correspondence to: Y. Zhang (yang_zhang@ncsu.edu)

Published by Copernicus Publications on behalf of the European Geosciences Union.

Title Page

Abstract

Introduction

Conclusions

References

Tables

Figures



Back

Close

Full Screen / Esc

Printer-friendly Version

Interactive Discussion



Abstract

Atmospheric chemistry plays a key role in determining the amounts and distributions of oxidants and gaseous precursors that control the formation of secondary gaseous and aerosol pollutants; all of those species can interact with the climate system. To understand the impacts of different gas-phase mechanisms on global air quality and climate predictions, in this work, a comprehensive comparative evaluation is performed using the Community Atmosphere Model (CAM) Version 5 with comprehensive tropospheric and stratospheric chemistry (CAM5-chem) within the Community Earth System Model (CESM) with two most commonly-used gas-phase chemical mechanisms: the 2005 Carbon Bond mechanism with Global Extension (CB05_GE) and the Model of OZone and Related chemical Tracers version 4 (MOZART-4) mechanism with additional updates (MOZART-4x). MOZART-4x and CB05_GE use different approaches to represent volatile organic compounds (VOCs) and different surrogates for secondary organic aerosol (SOA) precursors. MOZART-4x includes a more detailed representation of isoprene chemistry compared to CB05_GE. CB05_GE includes additional oxidation of SO₂ by O₃ over the surface of dust particles, which is not included in MOZART-4x. The results show that the two CAM5-chem simulations with CB05_GE and MOZART-4x predict similar chemical profiles for major gases (e.g., O₃, CO, and NO_x) compared to the aircraft measurements, with generally better agreement for NO_y profile by CB05_GE than MOZART-4x. The concentrations of SOA at four sites in CONUS and organic carbon (OC) over the IMPROVE sites are well predicted by MOZART-4x (with NMBs of -1.9 and 2.1 %, respectively) but moderately underpredicted by CB05_GE (with NMBs of -23.1 and -20.7 %, respectively). This is mainly due to the higher biogenic emissions and hydroxyl radical levels simulated with MOZART-4x than with CB05_GE. The concentrations of OC over Europe are largely underpredicted by both MOZART-4x and CB05_GE, with NMBs of -73.0 and -75.1 %, respectively, indicating the uncertainties in the emissions of precursors and primary OC and relevant model treatments such as the oxidations of VOCs and SOA formation. Uncertainties in the emissions and con-

GMDD

8, 7189–7247, 2015

CESM/CAM5 improvement and application

J. He et al.

Title Page

Abstract

Introduction

Conclusions

References

Tables

Figures



Back

Close

Full Screen / Esc

Printer-friendly Version

Interactive Discussion



vection scheme can contribute to the large bias in the model predictions (e.g., SO₂, CO, black carbon, and aerosol optical depth). The two simulations also have similar cloud/radiative predictions, with slightly better performance of domain average cloud condensation nuclei (CCN) at supersaturation of 0.5 % by CB05_GE, but slightly better agreement with observed CCN (at supersaturation of 0.2 %) profile over Beijing by MOZART-4x. The two gas-phase mechanisms result in a global average difference of 0.5 W m⁻² in simulated shortwave cloud radiative forcing, with significant differences (e.g., up to 13.6 W m⁻²) over subtropical regions.

1 Introduction

Atmospheric chemistry plays an important role in the perturbation of climate system by determining the amounts and distributions of important oxidants and gaseous precursors for secondary air pollutants such as ozone (O₃) and aerosols. Aerosols can influence the Earth's radiative balance by directly scattering and absorbing radiation and indirectly affecting cloud properties through acting as cloud condensation nuclei (CCN) and ice nuclei. The aerosol effects on radiation depend critically on their chemical composition and physical properties. Therefore, atmospheric chemistry is an important component for atmospheric and Earth system models. Different chemical mechanisms (e.g., different chemical reactions and kinetic parameters) can lead to differences in the predictions of gases, secondary aerosols, as well as climatic variables such as CCN, cloud droplet number concentration (CDNC), and radiative forcings (Luecken et al., 2008; Sarwar et al., 2008; Zhang et al., 2012a; Lamarque et al., 2013).

There are generally two types of species in the gas-phase mechanisms: inorganic and organic. Although most mechanisms include the same important inorganic species (e.g., O₃, CO, HO_x, and NO_x), the predicted amounts can vary greatly among different mechanisms (Knote et al., 2014a). Some mechanisms ignore reactions with very low reaction rates since they do not affect results significantly. Also, some reactions may use different rate coefficients with different dependence on atmospheric temper-

Title Page

Abstract

Introduction

Conclusions

References

Tables

Figures



Back

Close

Full Screen / Esc

Printer-friendly Version

Interactive Discussion



Pollution Research Center Mechanism (SAPRC99), and the CB05) can predict different O_3 concentrations up to 5 ppb at surface in July 2001. Knote et al. (2014a) also compared seven chemical mechanisms using a box model and found that the differences in daytime hydroxyl radical (OH) concentrations can be up to 40%.

Climate change can also strongly influence atmospheric chemistry and aerosols and therefore air quality. For example, photolysis and temperature-dependent reactions can be directly impacted by climate change (Jacob and Winner, 2009). Due to the nonlinear relationships between chemistry, aerosols, and climate, it is important to accurately represent their interactions in a three-dimensional global model. Several studies have demonstrated the capability of CAM-chem to represent tropospheric (Aghedo et al., 2011; Lamarque et al., 2010, 2011a, b; Tilmes et al., 2015) and stratospheric (Lamarque et al., 2008; Lamarque and Solomon, 2010) conditions. The chemical mechanism used in CAM-chem is based on MOZART-4, with detailed stratospheric chemistry of Kinnison et al. (2007). In this work, two most commonly used gas-phase mechanisms: the extended MOZART-4 (with updates as described by Knote et al. (2014b) and additional updates in this work) (referred to as MOZART-4x) and the CB05_GE chemical mechanisms are compared using the latest CESM/CAM5. The objectives are to examine the differences in the secondary organic aerosols (SOA) predictions resulted from the two gas-phase chemical mechanisms and study the sensitivity of air quality and climate predictions to different gas-phase chemical mechanisms.

2 Model descriptions

The CESM/CAM5 used in this work is based on CAM version 5.3 of CESM version 1.2.2, coupled to comprehensive tropospheric and stratospheric chemistry (CAM5-chem, Tilmes et al., 2015) using the 7-mode Modal Aerosol Model (MAM7) (Liu et al., 2012). This version of CAM5-chem was further developed and improved at North Carolina State University (NCSU) in collaboration with NCAR, as described below. A more

CESM/CAM5 improvement and application

J. He et al.

Title Page

Abstract

Introduction

Conclusions

References

Tables

Figures



Back

Close

Full Screen / Esc

Printer-friendly Version

Interactive Discussion



detailed description of this version of CESM CAM5-chem (referred to as CAM5-NCSU hereafter) used in this study can be found in He and Zhang (2014) and He et al. (2015).

2.1 Chemical mechanisms

In this study, CB05_GE has been updated to include additional kinetic reactions describing interactions between functionalization and fragmentation processes during gas-phase oxidation of anthropogenic and biogenic VOCs by OH (Glotfelty et al., 2015). The products of those reactions are linked with the organic gas/particle partitioning for SOA formation. Heterogeneous reactions on tropospheric aerosols and stratospheric clouds are also added as same as those in MOZART-4x (Tilmes et al., 2015) with one additional pathway in CB05_GE to simulate sulfate formation through oxidation of sulfur dioxide (SO₂) by O₃ on the surface of dust particles.

MOZART-4x used in this work extends the MOZART chemical mechanism used in Lamarque et al. (2012) and Tilmes et al. (2015) to include several updates as described in Knote et al. (2014b). These updates include (1) detailed treatments of monoterpenes (α -pinene, β -pinene, and limonene) and 2-methyl-3-buten-2-ol (MBO), (2) detailed treatments of aromatics (e.g., benzene, toluene, and xylenes), (3) additional glyoxal (C₂H₂O₂) production from oxidized VOCs products, and (4) an updated isoprene (ISOP) oxidation scheme. In this work, the oxidation of anthropogenic and biogenic VOCs and subsequent aging processes are also included in MOZART-4x, and the products of those reactions are linked with the organic gas/particle partitioning for SOA formation.

Table 1 shows the gas-phase organic precursors for SOA formation treated in MOZART-4x and CB05_GE. For aromatic precursors of SOA, MOZART-4x includes benzene, toluene (TOL), xylenes, and cresol. Although CB05_GE does not include benzene, it includes polycyclic aromatic hydrocarbons (PAH) as a SOA precursor. For alkane precursors of SOA, MOZART-4x includes BIGALK (lumped alkanes with carbon (C) number > 3), whereas CB05_GE includes ALKH (long-chain alkanes, with C > 6). For anthropogenic alkene precursors of SOA, MOZART-4x includes propene (C₃H₆)

CESM/CAM5 improvement and application

J. He et al.

Title Page

Abstract

Introduction

Conclusions

References

Tables

Figures



Back

Close

Full Screen / Esc

Printer-friendly Version

Interactive Discussion



and BIGENE (lumped alkenes with $C > 3$), whereas CB05_GE includes terminal olefin (OLE) and internal olefin (IOLE). The emissions for biogenic alkene precursors are from the Model of Emissions of Gases and Aerosols from Nature version 2.1 (MEGAN2.1, Guenther et al., 2012). Both MOZART-4x and CB05_GE include alpha-pinene (APIN), beta-pinene (BPIN), limonene, and ISOP as precursors for biogenic SOA. CB05_GE also includes additional biogenic precursors such as speciated ocimene (OCI), humulene (HUM) and terpinene (TER). However, in MOZART-4x, the species mapping for MEGAN emission calculation is slightly different. For example, α -pinene and other compounds (e.g., α -thujene, p-cymene, and o-cymene) are mapped into APIN, β -pinene and other compounds (e.g., sabinene and camphene) are mapped into BPIN, limonene and other compounds (e.g., phellandrene and terpinene) are mapped into LIMON, myrcene and other compounds (e.g., ocimene) are mapped into MYRC, and beta-caryophyllene and other sesquiterpenes (e.g., humulene and α -bergamotene) are mapped into BCARY. Due to the different mapping for MEGAN species, biogenic emissions between MOZART-4x and CB05_GE are different, which can result in different biogenic SOA predictions. On the other hand, the rate coefficients for the oxidations of biogenic VOCs (e.g., APIN, BPIN, and limonene) are constant in CB05_GE, whereas they are temperature dependent in MOZART-4x, such a difference can result in different SOA predictions as well. In addition, there are uncertainties in the HO_x recycling associated with isoprene chemistry in CB05_GE (Karamchandani et al., 2012), whereas MOZART-4x used in this work includes OH recycling from improved isoprene chemistry. For example, in CB05_GE, ISOP is oxidized by OH to generate 91.2% molar yield of the hydroperoxyl radical (HO_2). In MOZART-4x, the isoprene peroxy radical from the oxidation ISOP by OH (i.e., ISOPO₂) has different yields of HO_2 through reactions with NO, NO₃, methylperoxy radical (CH₃O₂), and acetylperoxy radical (CH₃CO₃), and it can also consume HO_2 itself. These reactions have different reaction rate coefficients. These differences can affect O₃, OH, and NO_x predictions, and thus the oxidation of VOCs.

**CESM/CAM5
improvement and
application**

J. He et al.

Title Page

Abstract

Introduction

Conclusions

References

Tables

Figures



Back

Close

Full Screen / Esc

Printer-friendly Version

Interactive Discussion



2.2 Aerosol/cloud treatments

In CAM5-NCSU, the aerosol module is based on MAM7 of Liu et al. (2012), with improvements in terms of condensation, nucleation, aerosol thermodynamics, and aerosol activation (He and Zhang, 2014; Gantt et al., 2014). The major updates include:

- (1) the new particle formation treatments with a combination of the default nucleation parameterizations of Vehkamäki et al. (2002), Merikanto et al. (2007), and a newly added ion-mediated aerosol nucleation (Yu, 2010) above the planetary boundary layer (PBL), and a combination of the three and an additional parameterization of Wang and Penner (2009) in the PBL,
- (2) the inorganic aerosol thermodynamics based on ISOR-ROPIA II of Fountoukis and Nenes (2007), which explicitly simulates the thermodynamics of sulfate (SO_4^{2-}), ammonium (NH_4^+), nitrate (NO_3^-), sodium (Na^+), and chloride (Cl^-) in the Aitken, accumulation, and fine sea-salt modes, as well as the impact of crustal species associated with the fine dust mode,
- (3) an advanced aerosol activation scheme based on Fountoukis and Nenes (2005) with additional updates based on Kumar et al. (2009) and Barahona et al. (2010), which accounts for adsorption activation from insoluble CCN and giant CCN equilibrium timescale on aerosol activation.

CAM5-NCSU also includes an advanced treatment for SOA formation based on a volatility-basis-set (VBS) approach that has been coupled with CB05_GE by Glotfelty et al. (2015) and is also coupled with MOZART-4x in this work. This approach consists of two primary components: (1) volatile SOA (VSOA) formation from anthropogenic VOCs (AVOCs) and biogenic VOCs (BVOCs) and (2) the volatility and aging of primary organic aerosol (POA) and the repartitioning of the semi/intermediate volatility compounds (S/IVOC) into SOA. The VSOA treatment is based on the treatment of Tsimpidi et al. (2010). The products of VOC oxidation are mapped onto the volatility distribution using the aerosol mass yields listed in Tsimpidi et al. (2010) using the CB05_GE species that represent those precursor VOCs. An additional pathway for the formation of SOA from PAH is also added in CB05_GE. The SOA mass yields for PAHs are derived from the laboratory measurements of Chan et al. (2009) following

GMDD

8, 7189–7247, 2015

CESM/CAM5 improvement and application

J. He et al.

Title Page

Abstract

Introduction

Conclusions

References

Tables

Figures



Back

Close

Full Screen / Esc

Printer-friendly Version

Interactive Discussion



**CESM/CAM5
improvement and
application**

J. He et al.

[Title Page](#)[Abstract](#)[Introduction](#)[Conclusions](#)[References](#)[Tables](#)[Figures](#)[Back](#)[Close](#)[Full Screen / Esc](#)[Printer-friendly Version](#)[Interactive Discussion](#)

the approach of Stainer et al. (2008), where the SOA mass yields for naphthalene, 1-methylnaphthalene, and 2-methylnaphthalene are averaged as surrogates for PAHs. The volatility of POA and the subsequent formation of SOA from POA vapors are based on the work of Robinson et al. (2007) and Shrivastava et al. (2008). POA emissions are distributed into nine logarithmically-spaced volatility bins with effective saturation (C^*) values ranging from 10^{-2} to $10^6 \mu\text{g m}^{-3}$. An updated emission spectrum is used to distribute the POA emissions into the volatility bins as the emission spectrum used in Robinson et al. (2007) has been shown to be too volatile (Cappa and Jimenez, 2010; Hodzic et al., 2010; Jathar et al., 2011). This new emission spectrum maps the anthropogenic POA emissions onto the volatility distribution based on thermodenuder measurements of gasoline exhaust and also contains separate emissions fractions for biomass burning aerosol which is less volatile than anthropogenic POA (May et al., 2013a, b). The emission spectrum of Robinson et al. (2007), also assumes that the emissions of SVOCs are fully captured by the original POA emissions and missing IVOCs are assumed to be equivalent to 1.5 times the POA emissions inventory with these additional emissions placed in the three highest volatility bins. However, because the estimations of the missing IVOC emissions are poorly constrained, the 1.5 times the POA mass for IVOCs is not included in this study.

In additional to the classic 1-D VBS treatment as described above, functionalization and fragmentation treatment described in Shrivastava et al. (2013) are included in this version of VBS for both VSOA and S/IVOCs (referred to as 1.5 D VBS). In this treatment, the VSOA and S/IVOCs in each volatility bin are split into three different species representing three generations of oxidation. During the first two generations of oxidation the mass of the VSOA and S/IVOCs grows by 15%, reflecting the addition of oxygen atoms. In this aging scheme not only do the masses of VSOA and S/IVOCs increase in generation when oxidized by OH (at a rate of 1.0×10^{-11} and $4.0 \times 10^{-11} \text{ cm}^3 \text{ molecule}^{-1} \text{ s}^{-1}$, respectively) but also their volatility decrease as they are moved into smaller volatility bins. Fragmentation occurs once the VSOA and S/IVOCs have aged to the third generation. This represents the breaking of carbon

bonds, which can increase volatility of the organic species thus reducing SOA formation. This is parameterized by allowing 17.25 % of the organic mass to pass to the next lowest volatility bin but passing 75 % of the VSOA and S/IVOC to the highest volatility bin in the VBS structure. The remaining mass is assumed to be lost to species of higher volatility than the VBS structure. A more detailed description of SOA formation from the VBS approach is summarized in Glotfelty et al. (2015).

3 Model configurations and evaluation protocols

3.1 Model setup and inputs

The simulations are performed with specified dynamics configuration, of which winds and temperature are driven by the Goddard Earth Observing System Model, Version 5 (GEOS-5) meteorology. The internally-derived meteorological fields are nudged every time step (30 min) by 10 % towards analysis fields from GEOS-5. The simulations are conducted for a 3 year period of 2008–2010 at a horizontal resolution of $0.9^\circ \times 1.25^\circ$ and a vertical resolution of 56 layers for CAM5. The initial chemical conditions are generated with same configurations with 1 year spinup.

The offline emissions used in this work are based on those used in Tilmes et al. (2015), of which the anthropogenic and biofuel emissions are from the Monitoring Atmospheric Composition and Climate/CityZen (MACCity) emission data set (Granier et al., 2011), and biomass burning emissions are taken from the Atmospheric Chemistry and Climate Model Intercomparison Project (ACCMIP) historical emissions dataset (Lamarque et al., 2010). The ACCMIP emissions are extrapolated for 2008–2010 with the Representative Concentration Pathway (RCP) 8.5 scenario and extended for VOCs and several other species for MOZART-4x species. MOZART-4x species are then mapped into CB05_GE species to generate emissions for CB05_GE species. The online emissions include biogenic VOCs from MEGAN2.1 (Guenther et al., 2012), light-

Title Page

Abstract

Introduction

Conclusions

References

Tables

Figures



Back

Close

Full Screen / Esc

Printer-friendly Version

Interactive Discussion



ning NO_x (Price and Rind, 1992; Price et al., 1997), mineral dust (Zender et al., 2003), and sea-salt (Martensson et al., 2003).

3.2 Available measurements for model evaluation

A number of observational datasets from surface networks and satellites are used for model evaluation. They are summarized along with the variables to be evaluated in Table 2. The global surface network includes data sets from the National Oceanic and Atmospheric Administration Climate Diagnostics Center (NOAA/CDC). The satellite datasets include the Moderate Resolution Imaging Spectroradiometer (MODIS) for the retrievals of cloud properties, the Clouds and Earth's Radiant Energy System (CERES), for the retrievals of radiation fluxes at surface and top of atmosphere, the Aura Ozone Monitoring Instrument in combination with Aura Microwave Limb Sounder (OMI/MLS) for the tropospheric ozone retrieval, the Measurements Of Pollution In The Troposphere (MOPITT) for tropospheric carbon monoxide (CO) retrieval, and the SCanning Imaging Absorption spectroMeter for Atmospheric CHartography (SCIAMACHY) for the retrievals of tropospheric nitrogen dioxide (NO_2), HCHO, and $\text{C}_2\text{H}_2\text{O}_2$. Other satellite-based data include the MODIS-derived CDNC and cloud liquid water path (LWP) by Bennartz (2007).

Regional observational networks include the Clean Air Status and Trends Network (CASTNET), the Interagency Monitoring of Protected Visual Environments (IMPROVE), the Speciation Trends Network (STN), and the Air Quality System (AQS) over CONUS; the European Monitoring and Evaluation Program (EMEP), the Base de Données sur la Qualité de l'Air (BDQA, France), and the European air quality database (AirBase) over Europe; the Ministry of Environmental Protection of China (MEPC), the National Institute for Environmental Studies of Japan (NIESJ), the Korean Ministry Of Environment (KMOE), and Taiwan Air Quality Monitoring Network (TAQMN) over East Asia. In addition to the data from the above networks, SOA measurements collected by Lewandowski et al. (2013) at four field study sites including Cleveland and Medina, OH

GMDD

8, 7189–7247, 2015

CESM/CAM5 improvement and application

J. He et al.

Title Page

Abstract

Introduction

Conclusions

References

Tables

Figures



Back

Close

Full Screen / Esc

Printer-friendly Version

Interactive Discussion



CESM/CAM5 improvement and application

J. He et al.

Title Page

Abstract

Introduction

Conclusions

References

Tables

Figures



Back

Close

Full Screen / Esc

Printer-friendly Version

Interactive Discussion



ing (SWCF), and longwave cloud forcing (LWCF) from CERES; cloud fraction (CF), aerosol optical depth (AOD), cloud optical thickness (COT), precipitating water vapor (PWV), and CCN from MODIS, as well as CDNC and LWP from Bennartz (2007). CDNC is calculated as an average value of layers between 850 and 960 hPa for comparison with the satellite-derived values. Chemical concentrations evaluated include CO, O₃, SO₂, ammonia (NH₃), NO₂, nitric acid (HNO₃), VOCs (i.e., formaldehyde, isoprene, and toluene), particulate matter (PM) with diameter less than and equal to 10 μm (PM₁₀) and 2.5 μm (PM_{2.5}), and PM_{2.5} major components (e.g., SO₄²⁻, NH₄⁺, NO₃⁻, black carbon (BC), organic carbon (OC), and total carbon (TC)) for CONUS and Europe. The chemical observations over East Asia are very limited, which only include surface observations of CO, SO₂, NO₂, and O₃ from Hong Kong, South Korea, and Japan, and PM₁₀ over mainland China (derived from air pollution index), Hong Kong, South Korea, and Japan. Since PM_{2.5} and PM₁₀ are not explicit species simulated in MAM7, they are simply assumed to be the particles in the first 5 modes (i.e., Aitken, accumulation, primary carbon, fine sea-salt, and fine dust modes) and the total 7 modes (i.e., Aitken, accumulation, primary carbon, fine sea-salt, fine dust, coarse sea-salt, and coarse dust modes), respectively. Column concentrations of tropospheric CO, NO₂, HCHO, C₂H₂O₂, and tropospheric O₃ residual (TOR) are evaluated for globe. The CO column evaluation follows the AMWG diagnostics approach, which applies 1° × 1° monthly mean Level 3 MOPITT a priori and averaging kernels to monthly mean model results to account for the a priori dependence and vertical resolution of the MOPITT data. The measured NO₂ and HCHO columns are derived from the satellite retrievals from SCIAMCHY, which are monthly mean gridded data on a 0.25° × 0.25° horizontal grid resolution for the period of 2008–2010. The measured glyoxal column is derived from the satellite retrievals from SCIAMCHY, which are monthly mean gridded data on a 0.125° × 0.125° horizontal grid resolution for the period of 2008. The measured O₃ is derived from the combining retrievals from the Aura Ozone Monitoring Instrument and Microwave Limb Sounder observations, which are monthly mean gridded data on a 1.25° × 1.25° horizontal grid resolution for the period of 2008–2010.

All surface observational data used for evaluating 2008–2010 simulations are available throughout 2008–2010 except for several variables with data during a limited time period of 2001–2010 including OC from EMEP, SOA from Lewandowski et al. (2013), and OA from Zhang et al. (2007) and Jimenez et al. (2009).

4 Results

4.1 Chemical evaluations

4.1.1 Surface evaluation

Table 3 summarizes the performance statistics for major chemical species for CAM5-NCSU simulations with MOZART-4x and CB05_GE. Figure 1 shows the scatter plots between observations and model results. The statistical performance of MOZART-4x and CB05_GE are similar for most chemical species. As shown in Table 3, CO is underpredicted over East Asia by both MOZART-4x and CB05_GE, with NMBs of -65.6 and -65.7 %, respectively. The underprediction of CO is mainly due to the underestimation of CO emissions from biomass burning (Tilmes et al., 2015). The underestimations in CO emissions lead to underpredictions of column CO concentrations, with NMBs of -25.8 and -24.4 % for MOZART-4x and CB05_GE, respectively. Both MOZART-4x and CB05_GE largely overpredict the concentrations of SO₂ over CONUS (with NMBs of 580.2 and 561.6 %, respectively), East Asia (with NMBs of 47.0 and 35.5 % , respectively), and Europe (with NMBs of 100.9 and 94.1 %, respectively), likely due to the overestimation of SO₂ emissions, the uncertainties in the emission injection heights as well as the vertical mixing scheme used. The overpredictions of surface SO₂ concentrations result in the overpredictions of the concentrations of SO₄²⁻ at the surface. Surface NH₃ concentrations from MOZART-4x and CB05_GE are overpredicted over Europe (with NMBs of 112.4 and 104.3 %, respectively), likely due to the overestimation of NH₃ emissions. The overpredictions of the NH₃ concentrations result in the

Title Page

Abstract

Introduction

Conclusions

References

Tables

Figures



Back

Close

Full Screen / Esc

Printer-friendly Version

Interactive Discussion



CESM/CAM5
improvement and
application

J. He et al.

Title Page

Abstract

Introduction

Conclusions

References

Tables

Figures



Back

Close

Full Screen / Esc

Printer-friendly Version

Interactive Discussion



overpredictions of the NH_4^+ concentrations at the surface. The concentrations of NO_2 from MOZART-4x and CB05_GE are largely underpredicted over Europe (with NMBs of -61.4 and -62.1% , respectively) and East Asia (with NMBs of -74.1 and -74.8% , respectively), which is likely due to the uncertainties in estimating total NO_x emissions and emission injection heights as well. As shown in Fig. 1, the concentrations of O_3 from MOZART-4x and CB05_GE are overpredicted over CONUS (with NMBs of 29.0 and 28.2% over the CASTNET sites, respectively), Europe (with NMBs of 19.3 and 22.2% over the EMEP sites, respectively) and East Asia (with NMBs of 68.8 and 65.7% over the KMOE sites, respectively). This is likely due to the less O_3 titration resulted from the underpredictions of NO_x , coarse resolution, as well as dilution of NO_x emissions. The overpredictions of SO_4^{2-} result in the underpredictions of NO_3^- and Cl^- , through thermodynamic equilibrium, and therefore overpredictions of HNO_3 over CONUS. However, HNO_3 is underpredicted over Europe, which is likely due to the underpredictions of NO_x . Cl^- is overpredicted over Europe, which is likely due to the uncertainties for the gas/particle partitioning over coarse modes (He and Zhang, 2014). Both MOZART-4x and CB05_GE predict $\text{PM}_{2.5}$ relatively well over CONUS, however, they underpredict PM_{10} over the AQS sites, with NMBs of -38.6 and -38.9% , respectively. The underpredictions of PM_{10} are likely due to the inaccurate predictions of coarse particles. Both MOZART-4x and CB05_GE underpredict $\text{PM}_{2.5}$ and PM_{10} over Airbase and BDQA sites, however, they overpredict PM_{10} by $3.14 \mu\text{g m}^{-3}$ (or by 22.2%) and $3.43 \mu\text{g m}^{-3}$ (or by 24.2%) over the EMEP sites, respectively, which is likely due to the overpredictions of coarse particles (e.g., Cl^-) over these sites. Both MOZART-4x and CB05_GE underpredict PM_{10} by $33.61 \mu\text{g m}^{-3}$ (or by 33.4%) and $26.71 \mu\text{g m}^{-3}$ (or by 26.6%) over the MEPC sites in mainland China, respectively, which is mainly due to the uncertainties in the emissions in primary gases (e.g., SO_2 , NO_x , NH_3 , and VOCs) and particulate species (e.g., SO_4^{2-} , BC, and POA). Granier et al. (2011) compared the regional emissions among different inventories and indicated large uncertainties in the emissions over China. For example, the differences of BC biomass burning emis-

sions over China among different inventories can be as large as a factor of 2.1, and the differences of SO_2 anthropogenic emissions can be as large as a factor of 1.8.

VOCs species such as HCHO, ISOP, and TOL are underpredicted over CONUS, likely due to the uncertainties in the biogenic emissions from MEGAN2.1, anthropogenic emissions (e.g., HCHO and TOL) and the chemical reactions as well as a coarse horizontal resolution used in this work. Both MOZART-4x and CB05_GE underpredict BC with NMBs of -29.3 and -29.3 %, respectively. The underpredictions of BC are likely due to the underestimations of BC emissions, as well as uncertainties in the transport and wet removal by convection (Ma et al., 2013; Wang et al., 2013; Tilmes et al., 2015).

OC is slightly overpredicted with an NMB of 2.1% by MOZART-4x over CONUS, whereas it is moderately underpredicted with an NMB of -20.7 % by CB05_GE. OC is evaluated against observations at the IMPROVE sites, and SOA dominates OC at these sites for both simulations with MOZART4-x and CB05_GE, with SOA/OC ratios of 83.0 and 59.6%, respectively. Although no SOA measurements are available from IMPROVE for evaluation, the differences in OC predictions can be attributed to the differences in SOA predictions because of dominances of SOA in total OC. Compared to the SOA observations at the four sites in the US from Lewandowski et al. (2013), MOZART-4x underpredicts SOA by $0.03 \mu\text{g m}^{-3}$ (or by 1.9%), whereas CB05_GE underpredicts SOA by $0.4 \mu\text{g m}^{-3}$ (or by 23.1%). Note that the SOA statistics are calculated using only four pairs of seasonal mean values at four sites in the US where the observed SOA data are available during 2008–2010; they therefore may not be representative because of limited data used for calculation. Figure 2 compares simulated and observed SOA concentrations at the four sites. MOZART-4x predicts higher SOA than CB05_GE at all four sites, which reduces underpredictions at Cleveland and Medina, OH but increases overpredictions at Bakersfield and Pasadena, CA. This indicates a better capability of MOZART-4x to simulate SOA at sites with relatively high SOA concentrations ($\geq 1 \mu\text{g m}^{-3}$) compared to CB05_GE despite its tendency of overpredictions at sites with lower SOA levels. The higher SOA concentrations predicted

GMDD

8, 7189–7247, 2015

CESM/CAM5 improvement and application

J. He et al.

Title Page

Abstract

Introduction

Conclusions

References

Tables

Figures



Back

Close

Full Screen / Esc

Printer-friendly Version

Interactive Discussion



to the uncertainties in the emissions of HCHO and its precursors as well as pathways for secondary HCHO formation. Both MOZART-4x and CB05_GE underpredict column glyoxal, with more underpredictions in CB05_GE. The underpredictions of glyoxal are mainly due to the uncertainties in the glyoxal chemical production and removal (Knote et al., 2014b). Several studies indicate that aromatics, isoprene, and ethyne are the major contributors to glyoxal formation (Washenfelder et al., 2011; Knote et al., 2014b). In MOZART-4x, glyoxal can be produced from photolysis of the oxidation products of toluene, and oxidation products of aromatics (e.g., benzene, toluene, and xylenes), isoprene, and ethyne. CB05_GE does not include pathways for glyoxal production through photolysis, but includes glyoxal production from oxidation of alkenes (e.g., OLE, IOLE, ethene, and ISOP) and aromatics (e.g., toluene and xylenes). Uncertainties in the emissions of these precursors and the production pathways can propagate into the predicted glyoxal concentrations. MOZART-4x includes additional pathways for glyoxal production through photolysis and improved treatments for glyoxal production from additional oxidized VOCs (e.g., benzene) products (Knote et al., 2014b), which can result in higher glyoxal than in CB05_GE. The major chemical loss of glyoxal includes photochemical loss and oxidation by OH. The uncertainties in OH levels can propagate into glyoxal predictions as well. In addition, CB05_GE includes an additional pathway for glyoxal loss through its uptake by aerosols, which is not included in MOZART-4x. This can explain in part the lower glyoxal concentrations predicted by CB05_GE than by MOZART-4x. An advanced treatment for glyoxal formation should be therefore developed in the future. Both MOZART-4x and CB05_GE overpredict column NO₂, likely due to the uncertainties in the NO₂ aircraft emissions and overpredictions of lightning NO_x. The lightning NO_x emissions are calculated online (i.e., 6.2 and 6.4 TgNyr⁻¹ in CB05_GE and MOZART-4x, respectively), which is about 1.2–2.2 TgNyr⁻¹ higher than that in Lamarque et al. (2012) and Tilmes et al. (2015). Tilmes et al. (2015) have shown that increased lightning NO_x emissions in CAM-chem can lead to an increase in OH levels and therefore a decrease in the lifetime of methane and an underestimation of CO in the model. The higher zonal-mean concentrations of NO₂ in CB05_GE than

**CESM/CAM5
improvement and
application**

J. He et al.

Title Page

Abstract

Introduction

Conclusions

References

Tables

Figures



Back

Close

Full Screen / Esc

Printer-friendly Version

Interactive Discussion



those in MOZART-4x are likely due to additional NO₂ production from the reactions of VOCs with NO₃ radical in CB05_GE (e.g., reactions of NO₃ with OLE, IOLE, and ethene). The zonal-mean distribution of summer TOR from CB05_GE is similar to that from MOZART-4x. TOR is overpredicted over 40° S–50° N, and underpredicted over 40–60° S. The higher TOR from CB05_GE is mainly due to higher O₃ production from higher NO₂ and lower O₃ loss from lower OH in CB05_GE than in MOZART-4x.

4.1.3 Vertical profile evaluation

Figure 4 compares the vertical profiles of major gases against the aircraft observations (i.e., ARCPAC, ARCTAS, START08, and CalNex). Compared with aircraft measurements, MOZART-4x and CB05_GE predict similar O₃ and CO profiles, whereas there are large differences in NO_x (above 9 km) and NO_y profiles (below 12 km). O₃ profiles from MOZART-4x and CB05_GE overall agree well with aircraft measurements, although O₃ is slightly overpredicted near the surface. As discussed previously, the significant underpredictions of CO profiles in both MOZART-4x and CB05_GE are mainly due to the underestimations of CO biomass burning emissions and uncertainties in OH predictions. Both MOZART-4x and CB05_GE underpredict the vertical concentrations of NO_x at higher altitudes (e.g., above 9 km in ARCTAS and STRAT08), with a slightly better agreement in CB05_GE than in MOZART-4x. The concentrations of NO_x near the surface are slightly overpredicted by both simulations. The underpredictions of the concentrations of NO_x at higher altitudes are likely due in part to the uncertainties in the NO_x emissions, the chemical reactions of nitrogen cycles (e.g., heterogeneous reactions of NO₂, NO₃, and N₂O₅ over the surface of aerosol particles), the convection scheme, as well as the aircraft campaign data. Some field campaigns (e.g., ARCPAC) focus on the polluted regions with a significant contribution from biomass burning and local sources (Tilmes et al., 2015). The underestimations of emissions from these sources and uncertainties in the vertical mixing scheme can result in the underpredictions of their profiles. NO_y includes all the reactive nitrogen species. The simulated NO_y profiles from CB05_GE agree better with those observed during APCPAC, ARC-

Title Page

Abstract

Introduction

Conclusions

References

Tables

Figures



Back

Close

Full Screen / Esc

Printer-friendly Version

Interactive Discussion



TAS, and CalNex than those from MOZART-4x, whereas MOZART-4x predicts slightly better NO_y profile against START08 in the lower troposphere than CB05_GE. Figure 5 compares the vertical profile of simulated CCN against the aircraft observations from CCN_China. Both MOZART-4x and CB05_GE slightly overpredict CCN (at supersaturation of 0.2 %) profile over Beijing area, with less overpredictions in MOZART-4x.

4.2 Column comparisons

Figure 6a and b compares the column mass abundance of major gaseous and aerosol species simulated by MOZART-4x and CB05_GE. As shown in Fig. 6a, column CO predicted by MOZART-4x is about $2.4 \times 10^{20} \text{ m}^{-2}$ (or by 2.3 %) lower than that by CB05_GE in the global mean. The different column CO concentrations are due to different pathways for chemical production and loss of CO and different OH levels between MOZART-4x and CB05_GE. The chemical production of CO is mainly from photolysis and oxidation of VOCs species, and the chemical loss of CO is mainly from the oxidation by OH. Different concentrations of VOCs species can result in different chemical production of CO. Meanwhile, the only chemical loss of CO in CB05_GE is the oxidation of CO by OH, which produces HO_2 and CO_2 . Higher OH levels in MOZART-4x can result in more CO loss. MOZART-4x includes an additional loss pathway of CO oxidized by OH to produce CO_2 and H. As a result, the combined rate constant for both pathways of CO oxidation by OH in MOZART-4x is about 4 % higher than in CB05_GE. All these differences result in 2301 and 2265 Tgyr^{-1} chemical loss of CO in MOZART-4x and CB05_GE, respectively.

The global mean differences in the simulated column concentrations of SO_2 and NH_3 between MOZART-4x and CB05_GE are $2.0 \times 10^{18} \text{ m}^{-2}$ (or by 12.5 %) and $1.9 \times 10^{17} \text{ m}^{-2}$ (or by 3.1 %), respectively. The lower column abundance of SO_2 in CB05_GE is mainly due the additional pathway for SO_2 loss through oxidation by O_3 over the surface of dust particles, which is not include in MOZART-4x. This pathway can produce more SO_4^{2-} and therefore, more NH_3 is partitioned into the particulate phase to

[Title Page](#)[Abstract](#)[Introduction](#)[Conclusions](#)[References](#)[Tables](#)[Figures](#)[⏪](#)[⏩](#)[◀](#)[▶](#)[Back](#)[Close](#)[Full Screen / Esc](#)[Printer-friendly Version](#)[Interactive Discussion](#)

CESM/CAM5 improvement and application

J. He et al.

Title Page

Abstract

Introduction

Conclusions

References

Tables

Figures



Back

Close

Full Screen / Esc

Printer-friendly Version

Interactive Discussion



form NH_4^+ which can neutralize additional SO_4^{2-} , resulting in lower column abundance of NH_3 in CB05_GE. Both column concentrations of NO_x and NO_y from MOZART-4x are about $9.4 \times 10^{17} \text{ m}^{-2}$ (or by 9.5 %) and $3.6 \times 10^{19} \text{ m}^{-2}$ (or by 46.3 %) lower than that from CB05_GE. The higher NO_x in CB05_GE is mainly due to the lower OH available for the chemical loss through the reaction of NO_2 with OH. NO_y in MOZART-4x includes NO_x , nitrate radical (NO_3), nitrogen pentoxide (N_2O_5), HNO_3 , peroxyacetic acid (HO_2NO_2), chlorine nitrate (ClONO_2), bromine nitrate (BrONO_2), peroxyacetyl nitrate (PAN), organic nitrate (ONIT), methacryloyl peroxyacetyl nitrate (MPAN), peroxy radical from the reaction of NO_3 with ISOP (ISOPNO3), and lumped isoprene nitrate (ONITR), whereas NO_y in CB05_GE includes NO_x , NO_3 , N_2O_5 , HNO_3 , HO_2NO_2 , ClONO_2 , BrONO_2 , nitrous acid (HONO), PAN, higher peroxyacyl nitrates (PANX), and organic nitrate (NTR). The reactions for reactive nitrogen species are different in MOZART-4x and CB05_GE, resulting in different NO_y predictions.

The tropospheric column O_3 from MOZART-4x is about 1.5 DU (or by 4.7 %) lower than that from CB05_GE. Table 4 shows the tropospheric O_3 budget from MOZART-4x and CB05_GE. The burdens of tropospheric O_3 from MOZART-4x and CB05_GE are 325 and 333 Tg, respectively, which is comparable to the previous studies using CAM (Lamarque et al., 2012; Young et al., 2013). The O_3 burden from MOZART-4x in this work is about 12 Tg (or 3.8 %) higher than that in Tilmes et al. (2015), which is mainly due to the additional kinetic reactions included in this version of MOZART-4x. The dry deposition flux of O_3 from MOZART-4x is 679 Tgyr^{-1} , which is about 3.7 % lower than that from CB05_GE (i.e., 705 Tgyr^{-1}). The lower O_3 dry deposition flux is mainly due to the lower O_3 concentration simulated by MOZART-4x. The O_3 chemical production and loss from CB05_GE and MOZART-4x are roughly within the range of Young et al. (2013). The O_3 chemical production from MOZART-4x is comparable to that of Lamarque et al. (2012), but the O_3 chemical production from CB05_GE is about 12.8 % higher than Lamarque et al. (2012). In this table, chemical production is calculated mainly from reactions of NO with peroxy radicals and chemical loss is calculated mainly from the oxygen radical in the reaction of excited oxygen atom (O^1D) with water

CESM/CAM5 improvement and application

J. He et al.

Title Page

Abstract

Introduction

Conclusions

References

Tables

Figures



Back

Close

Full Screen / Esc

Printer-friendly Version

Interactive Discussion



vapor (H_2O) and from the reactions of O_3 with the HO_2 , OH, and alkenes. Different peroxy radicals and alkenes treated and different reaction rates used in the two mechanisms can contribute to the different chemical production and chemical loss of O_3 . The O_3 lifetime is calculated based on the ratio of O_3 burden to the total O_3 loss (dry deposition + chemical loss). The O_3 lifetime from CB05_GE is comparable to those reported by Young et al. (2013), and the O_3 lifetime from MOZART-4x is comparable to those reported by Lamarque et al. (2012) and Tilmes et al. (2015).

Column concentrations of OH, HCHO, and ISOP from MOZART-4x are higher than CB05_GE, with global mean values of $9.7 \times 10^{13} \text{ m}^{-2}$ (or by 0.8 %), $3.5 \times 10^{17} \text{ m}^{-2}$ (or by 1.3 %), and $1.1 \times 10^{18} \text{ m}^{-2}$ (or by 25.6 %), respectively. The higher column concentrations of OH and HCHO are likely due to the photolysis of more peroxide species, better HO_x recycling, and higher precursors for secondary HCHO (e.g., ISOP) in MOZART-4x. MOZART-4x includes detailed organic peroxide species, whereas in CB05_GE, all the organic peroxide species are lumped into one species (i.e., ROOH). The uncertainties in HO_x recycling in CB05_GE can also result in uncertainties in OH predictions. The higher ISOP is mainly due to higher biogenic emissions and less chemical loss in MOZART-4x than that in CB05_GE. In MOZART-4x, the chemical loss of ISOP is mainly from the oxidation of ISOP by OH, O_3 , and NO_3 . However, in CB05_GE, the chemical loss of ISOP includes not only the oxidation of ISOP by OH, O_3 , and NO_3 , but also the consumption of ISOP by atomic oxygen (i.e., O), NO_2 , and chlorine (Cl).

As shown in Fig. 6b, the differences in the domain average column mass abundances of most aerosol species (e.g., NH_4^+ , BC, Cl^- , and POA) between MOZART-4x and CB05_GE are within $\pm 0.02 \text{ mg m}^{-2}$. The differences in the column SO_4^{2-} vary from -25.2 to 0.4 mg m^{-2} , with the global mean of -0.2 mg m^{-2} . The simulated column concentrations of SO_4^{2-} from MOZART-4x are much lower than those from CB05_GE over East Asia, western Europe, and Middle Africa. SO_2 can be oxidized by O_3 to form SO_4^{2-} on the surface of dust particles in CB05_GE, which explains additional formation of SO_4^{2-} by CB05_GE over these regions. The differences of the spatial distributions

**CESM/CAM5
improvement and
application**

J. He et al.

Title Page

Abstract

Introduction

Conclusions

References

Tables

Figures



Back

Close

Full Screen / Esc

Printer-friendly Version

Interactive Discussion



predicted by MOZART-4x and CB05_GE are about 17–44, and 10–47 %, respectively, with South America the least and East Asia the most. The contributions of BSOA to TSOA predicted by MOZART-4x and CB05_GE are about 31–75, and 26–76 %, respectively, with East Asia the least and South America the most. The contribution of GLSOA to TSOA predicted by CB05_GE is about 2–6 %. CB05_GE used in this work includes a simple conversion of glyoxal to condensable VOCs, which can be up-taken by preexisting particles to form SOA. However, this conversion is not included in MOZART-4x. Therefore, there is no GLSOA predicted by MOZART-4x despite it predicts higher glyoxal as shown in Fig. 3. The contributions of SVSOA to TSOA predicted by MOZART-4x and CB05_GE are about 8–37, and 8–41 %, respectively, with South America the least and South Africa the most. Among four types of SOA, both MOZART-4x and CB05_GE predict BSOA as the main contributor over most regions (e.g., Australia, North America, South Africa, and South America) and ASOA as the main contributor over East Asia, which is mainly due to the much higher anthropogenic emissions over East Asia. Europe is a different example. MOZART-4x predicts BSOA as the top contributor (44 %) and ASOA as the second largest contributor (40 %), whereas CB05_GE predicts ASOA as the top contributor (45 %) and BSOA as the second largest contributor (36 %). Both MOZART-4x and CB05_GE predict ASOA as the top contributor (46–59 %) for spring, fall, and winter, and BSOA as the top contributor (57 and 47 %, respectively) for summer over Europe. Since MOZART-4x predicts higher BSOA than CB05_GE, BSOA is dominant in MOZART-4x on the annual average. The higher BSOA from MOZART-4x than CB05_GE is mainly due to the higher BVOCs emissions and higher OH levels in MOZART-4x. The total BVOCs emission in MOZART-4x is about $2.5 \times 10^{-3} \text{ kg m}^{-2} \text{ yr}^{-1}$, which is about $7.2 \times 10^{-5} \text{ kg m}^{-2} \text{ yr}^{-1}$ (or 2.9 %) higher than CB05_GE. The higher BVOCs emissions in MOZART-4x are mainly due to the different species mapping for MEGAN emission calculations. The differences of SOA from biogenic alkenes between MOZART-4x and CB05_GE are MYRC and BCARY in MOZART-4x, and OCI, HUM, and TER in CB05_GE (as shown in Table 1). In CAM-chem that uses MOZART, MEGAN calculates all of the individual

**CESM/CAM5
improvement and
application**

J. He et al.

Title Page

Abstract

Introduction

Conclusions

References

Tables

Figures



Back

Close

Full Screen / Esc

Printer-friendly Version

Interactive Discussion



species and CAM-chem sums them up to map with the MOZART mechanism species. For example, MYRC emissions consist of myrcene and ocimene, BCARY emissions consist of beta-caryophyllene, alpha-bergamotene, beta-bisabolene, beta-farnescene, and alpha-humulene, and LIMON emissions consist of limonene, phellandrene, and terpinene. Therefore, the biogenic emissions for more types of VOCs in MOZART-4x are higher than those in CB05_GE, resulting in higher BSOA in MOZART-4x. The differences in SOA from aromatics between MOZART-4x and CB05_GE are BENZENE in MOZART-4x and PAH in CB05_GE (as shown in Table 1). The emissions of PAH are higher over Europe, East Asia, eastern US, and South Africa. The benzene emissions are about 1 order of magnitude higher than the emissions of PAH, and the rate constant of the oxidation of benzene by OH is temperature dependent whereas it is constant for oxidation of PAH by OH. In addition, OH levels are higher in MOZART-4x than those in CB05_GE. These differences could result in different ASOA between two simulations. Both MOZART-4x and CB05_GE predict higher SVSOA contributions over South Africa than other regions, which is mainly due to the higher POA emissions (e.g., biomass burning) over this region.

Although the percentage contributions of different types of SOA predicted by MOZART-4x and CB05_GE are similar over most regions, the absolute mass concentrations of different types of SOA are different. For example, TSOA predicted by MOZART-4x is about $0.02\text{--}2.0\text{ mg m}^{-2}$ higher than by CB05_GE over these regions. ASOA predicted by MOZART-4x is about $0.068\text{--}1.017\text{ mg m}^{-2}$ higher than predicted by CB05_GE over most regions except Europe (0.054 mg m^{-2} lower) and East Asia (0.062 mg m^{-2} lower). BSOA predicted by MOZART-4x is about $0.162\text{--}1.365\text{ mg m}^{-2}$ higher than predicted by CB05_GE over most regions except Australia (0.003 mg m^{-2} lower). MOZART-4x includes SOA formation from benzene, which can predict higher ASOA formation. In addition, OH predicted by MOZART-4x is higher than CB05_GE (see Fig. 6a), which can produce more condensable SOA gaseous precursors through oxidations of VOCs. The higher BVOCs emissions in MOZART-4x due to different map-

ping for MEGAN species can also contribute to the higher BSOA formation in MOZART-4x.

4.4 Evaluations of cloud/radiative predictions

Table 5 shows the statistical performance for major cloud/radiative variables for MOZART-4x and CB05_GE simulations. Radiative variables such as OLR, FSDS, and FLDS show excellent agreement with observations, with NMBs within $\pm 8\%$ for both simulations. However, SWCF is overpredicted by both MOZART-4x and CB05_GE, with NMBs of 26.4 and 27.7%, respectively, and LWCF is underpredicted by both MOZART-4x and CB05_GE, with NMBs of -21.6 and -16.7% , respectively. All predicted radiative variables show high correlation with observations, with correlation coefficients of 0.9 to 0.99. CF is well predicted by MOZART-4x, with an NMB of 6.3%, whereas CCN5, CDNC, COT, and LWP are moderately overpredicted or underpredicted, with NMBs of -32.1 , 19.7, -26.0 , and 2.8%, respectively. The performance of cloud variables is similar in CB05_GE, with NMBs of 6.0, -29.0 , 20.8, -26.0 , and 1.7% for CF, CCN5, CDNC, COT, and LWP, respectively. AOD is also underpredicted by both MOZART-4x and CB05_GE, with NMBs of -23.9 and -24.6% , respectively.

Figure 8 shows the Taylor diagram (Taylor, 2001) comparing the model performance of MOZART-4x with that of the CB05_GE for cloud and radiative predictions. The similarity between the two patterns is quantified in terms of their correlations (i.e., angle), their standard deviations (i.e., y axis), and the ratio of their variances (i.e., x axis). In general, the performance of major cloud/radiative variables between MOZART-4x and CB05_GE are similar. The major differences in the performance of cloud/radiative variables between MOZART-4x and CB05_GE are the variances of CCN5, CDNC, and SWCF, which is mainly due to the predicted aerosol distributions (see Fig. 6b). The larger deviation of COT and LWP from observations (i.e., the two points located outside the diagram in Fig. 8) suggests the uncertainties both in the model treatments for cloud dynamics and thermodynamics as well as in the satellite retrievals.

Title Page

Abstract

Introduction

Conclusions

References

Tables

Figures



Back

Close

Full Screen / Esc

Printer-friendly Version

Interactive Discussion



Due to the underpredictions of cloud variables (e.g., COT and CCN5), OLR is slightly overpredicted by 7.8 W m^{-2} (or by 3.6 %), and LWCF is underpredicted by 4.8 W m^{-2} (or by 21.6 %) in MOZART-4x. Similarly, OLR is slightly overpredicted by 6.7 W m^{-2} (or by 3.1 %) and LWCF is underpredicted by 3.7 W m^{-2} (or by 16.7 %) in CB05_GE. Figure 9 shows the comparisons of satellite observations with model predictions for AOD, CCN5, CDNC, COT, and SWCF averaged during 2008–2010. The underpredictions of AOD over oceanic areas can be attributed to the uncertainties in the sea-salt emissions and inaccurate predictions of other PM components (e.g., marine organic aerosols) over the ocean and overestimation of oceanic AOD in the MODIS collection 5.1 (Levy et al., 2013). The underprediction of AOD over land (e.g., tropical islands) is mainly due to the significant underestimation of biomass burning emissions in the model (Tilmes et al., 2015). AOD is higher in MOZART-4x over most land areas (except East Asia and Europe) than in CB05_GE. The higher AOD in MOZART-4x is mainly due to higher SOA (e.g., over most land areas) and higher NO_3^- (e.g., over CONUS) in MOZART-4x. The lower AOD over East Asia and Europe in MOZART-4x is mainly due to the lower SO_4^{2-} as there is an additional pathway of SO_2 (oxidized by O_3) included in CB05_GE but it is not included in MOZART-4x and lower NH_4^+ to neutralize lower SO_4^{2-} through thermodynamic equilibrium. This additional pathway also results in higher H_2SO_4 predictions in CB05_GE and higher aerosol number concentration through homogeneous nucleation. Therefore, CCN5 is higher in CB05_GE than in MOZART-4x (see Fig. 9). CDNC is moderately overpredicted for both cases. Cloud droplet formation is sensitive to both particle number concentrations and updraft velocity (Reutter et al., 2009). The overprediction of CDNC is due partly to high activation fractions (e.g., inclusion of adsorption activation from insoluble CCN and effective uptake coefficient of 0.06 used in this work) (Gantt et al., 2014) as well as the uncertainties in the model treatments for cloud microphysics (e.g., resolved clouds and subgrid-scale cumulus clouds) and satellite retrievals (e.g., error propagation of the input variables to derive CDNC) (Bernartz, 2007). COT is largely overpredicted over Southeast Asia and South America and underpredicted over polar regions for both simulations. Overpredictions in CDNC and

GMDD

8, 7189–7247, 2015

CESM/CAM5 improvement and application

J. He et al.

Title Page

Abstract

Introduction

Conclusions

References

Tables

Figures



Back

Close

Full Screen / Esc

Printer-friendly Version

Interactive Discussion



COT can increase cloud albedo and therefore, increase SWCF over the low and middle latitudes. The large underpredictions of COT over polar regions can be attributed to the uncertainties in plane-parallel visible-near-infrared retrievals with low solar zenith angle (Seethala and Horváth, 2010) and the influence of radiatively active snow on overlying cloud fraction (Kay et al., 2012). Due to the different gas-phase mechanisms, the predicted SWCF (Fig. 9) and LWCF (Figure not shown) are different, with a global average difference of 0.5 and 1.1 W m^{-2} , respectively. However, the absolute differences in simulated SWCF can be as large as 13.6 W m^{-2} as shown in Fig. 9. The large differences of SWCF and LWCF between MOZART-4x and CB05_GE are mainly over subtropical regions (e.g., 20° S–20° N), which is mainly due to lower COT in MOZART-4x than in CB05_GE.

5 Conclusions

In this work, MOZART-4x and CB05_GE are coupled with CAM5-NCSU. MOZART-4x uses lumped species approach to represent organic chemistry whereas CB05_GE uses lumped structure approach. MOZART-4x and CB05_GE include different surrogates for SOA precursors, which can result in different SOA predictions. MOZART-4x includes HO_x recycling associated with improved isoprene chemistry whereas CB05_GE contains simpler isoprene chemistry, which can result in different OH and isoprene predictions and thus, SOA predictions. CB05_GE includes additional oxidation of SO_2 by O_3 over the surface of dust particles to produce additional SO_4^{2-} , which is not included in MOZART-4x. These differences can result in different secondary gaseous and aerosol predictions.

The comparisons between the two gas-phase mechanisms are conducted in terms of chemical and cloud/radiative predictions. Predictions of major gases and inorganic aerosols predicted by MOZART-4x and CB05_GE are overall similar. Significant differences in some species (e.g., NO_y , glyoxal, and SOA) predictions are mainly due to the different reaction pathways treated in the two mechanisms. Large biases exist for sur-

GMDD

8, 7189–7247, 2015

CESM/CAM5 improvement and application

J. He et al.

Title Page

Abstract

Introduction

Conclusions

References

Tables

Figures



Back

Close

Full Screen / Esc

Printer-friendly Version

Interactive Discussion



CESM/CAM5 improvement and application

J. He et al.

Title Page

Abstract

Introduction

Conclusions

References

Tables

Figures



Back

Close

Full Screen / Esc

Printer-friendly Version

Interactive Discussion



face SO₂, CO, and NH₃ predictions against available observations, which is likely due to the uncertainties in the emissions or emission injection heights. Several studies indicate that the uncertainties in regional emissions (e.g., BC and SO₂) can be expected to be as large as a factor of 2 or larger (Bond et al., 2007; Smith et al., 2011). Large discrepancies still remain for major species such as SO₂, NO_x, BC, and CO among different inventories (Granier et al., 2011). Both MOZART-4x and CB05_GE overpredict surface O₃ over CONUS, Europe, and East Asia, which is due in part to less O₃ titration resulted from underpredictions of NO_x, the use of a coarse grid resolution, as well as dilution of NO_x emissions. The overpredictions of SO₂ and NH₃ result in the overpredictions of SO₄²⁻ and NH₄⁺ over CONUS and Europe. Both surface CO and column CO are underpredicted, which is mainly due to underestimations in the CO emissions from biomass burning and possible uncertainties in the OH production. Surface SO₂ is overpredicted whereas column SO₂ is underpredicted, indicating the uncertainties in the vertical mixing scheme or emission injection heights as reported in East Asia (Zhang et al., 2015a, b). The large underpredictions of column glyoxal are mainly due to the uncertainties in the chemical production and loss for glyoxal. Tropospheric O₃ predicted by MOZART-4x is about 4.7 % lower than CB05_GE, but agrees better with OMI/MLS. The lower column O₃ in MOZART-4x is mainly due to lower NO₂ and higher OH in MOZART-4x. The column SOA predicted by MOZART-4x is about 8.4 % higher than CB05_GE, whereas there is not much difference for column POA. The difference in SOA column is mainly due to higher BVOCs emissions and higher OH levels in MOZART-4x than in CB05_GE. Chemical profiles (e.g., O₃, CO, and NO_x) predicted by CB05_GE and MOZART-4x are overall similar, whereas NO_y profile predicted by CB05_GE agree better with aircraft measurements than by MOZART-4x.

The concentrations of VOCs (e.g., formaldehyde, isoprene, and toluene) are moderately to largely underpredicted, which is likely due to the use of a coarse grid resolution, the uncertainties in the biogenic emissions, as well as chemical reactions (e.g., reaction rate coefficients for HCHO production and loss and isoprene chemistry). The concentration of OC over CONUS is well predicted by MOZART-4x, with an NMB of 2.1 %, 25

CESM/CAM5 improvement and application

J. He et al.

Title Page

Abstract

Introduction

Conclusions

References

Tables

Figures



Back

Close

Full Screen / Esc

Printer-friendly Version

Interactive Discussion



whereas it is moderately underpredicted by CB05_GE, with an NMB of -20.7% . Compared to the observations at the four sites in the US from Lewandowski et al. (2013), SOA is well predicted by MOZART-4x, with an NMB of -1.9% , whereas it is moderately underpredicted by CB05_GE, with an NMB of -23.1% , indicating a better capability to predict SOA over these sites by MOZART-4x despite its tendency to overpredict SOA concentrations at sites with low SOA levels such as Bakersfield and Pasadena, CA. However, the concentrations of OC over Europe is largely underpredicted by both MOZART-4x and CB05_GE, with NMBs of -74.2 and -75.1% , respectively, indicating the uncertainties in the emissions, chemical reactions, as well as SOA formation treatment. Both MOZART-4x and CB05_GE largely underpredict HOA in the Northern Hemisphere, with NMBs of -77.2 and -76.7% , respectively, indicating the uncertainties in the POA evaporation treatment as well as POA emissions. OOA is also underpredicted by both MOZART-4x and CB05_GE in the Northern Hemisphere, with NMBs of -56.5 and -62.3% , respectively, indicating the uncertainties in the emissions, fragmentation rates, as well as SOA formation treatment. $PM_{2.5}$ is well predicted over CONUS by both MOZART-4x and CB05_GE, with NMBs of 0.7 and -1.1% , respectively, whereas it is moderately underpredicted over Europe, with NMBs of -39.8 and -37.4% , respectively. The underpredictions of $PM_{2.5}$ over Europe are mainly due to the inaccurate predictions of OA over Europe. PM_{10} is underpredicted over CONUS, Europe, and East Asia by both MOZART-4x and CB05_GE, which is mainly due to the inaccurate predictions of coarse particles and uncertainties in the anthropogenic emissions (e.g., SO_2 , BC, and OC) and online dust and sea-salt emissions. The different AOD predictions between CB05_GE and MOZART-4x are mainly due to the different predictions in SOA, SO_4^{2-} , NH_4^+ , NO_3^- , and dust concentrations.

The cloud/radiative predictions from the two simulations are also similar, with slightly better domain average performance of CCN5, LWP, and LWCF in CB05_GE. But MOZART-4x predicts slightly better CCN profile over Beijing than CB05_GE compared to aircraft measurements. The different gas-phase mechanisms result in different predictions in aerosols and clouds, and therefore, a domain average difference

CESM/CAM5 improvement and application

J. He et al.

Title Page

Abstract

Introduction

Conclusions

References

Tables

Figures



Back

Close

Full Screen / Esc

Printer-friendly Version

Interactive Discussion



of 0.5 W m^{-2} in simulated SWCF, which can be as large as 13.6 W m^{-2} over subtropical regions. Such differences are caused by different aerosol and cloud predictions from both simulations. Radiative variables such as OLR, FSDS, and FLDS, show excellent agreement with observations, with NMBs within $\pm 8\%$ for both MOZART-4x and CB05_GE. However, there are large deviations for COT and LWP, indicating the uncertainties both in the model treatments for cloud dynamics and thermodynamics and in the satellite retrievals.

In summary, MOZART-4x and CB05_GE differ in their approaches to represent VOCs and surrogates for SOA precursors. MOZART-4x includes a more detailed representation of isoprene chemistry compared to CB05_GE. Based on the above comparisons of simulations using both mechanisms and evaluation against available measurements in this study, MOZART-4x with the 1.5 D VBS SOA module in CESM-NCSU generally gives a better agreement with observations for surface concentrations of O_3 over Europe, HNO_3 , HCHO, ISOP over CONUS, SOA, SO_4^{2-} , NO_3^- , and NH_4^+ over CONUS and Europe, and column mass abundances of HCHO, CH_2O_2 , SO_2 , and O_3 , whereas CB05_GE generally gives a better agreement for surface concentrations of SO_2 , NH_3 , O_3 over CONUS and East Asia, HNO_3 over Europe, $\text{PM}_{2.5}$ and PM_{10} over Europe, PM_{10} over East Asia, vertical profiles of NO_y , and column mass abundances of CO. Both simulations give predictions of cloud/radiative variables with slightly better domain average performance of CCN5, LWP, and LWCF in CB05_GE.

Acknowledgements. This work is sponsored by the U.S. National Science Foundation EaSM program AGS-1049200 and NCAR Advanced Study Program. MODIS data and CERES data are provided by NASA via <http://ladsweb.nascom.nasa.gov/data/search.html> and http://ceres.larc.nasa.gov/order_data.php, respectively. CDNC data are provided by Ralf Bennartz. Other surface network data were downloaded from their respective web sites. ARCPAC and CalNex data are from NOAA, STRAT08 data are from NCAR, ARCTAS data are from NASA, CCN_China are from Zhang et al. (2011), and SOA data of Lewandowski et al. (2013) are provided by Tadeusz Kleindienst, U.S. EPA. We would like to acknowledge high-performance computing support from Yellowstone (ark:/85065/d7wd3xhc) provided by NCAR's Computational and Information Systems Laboratory, sponsored by the U.S. National Science Founda-

tion. The National Center for Atmospheric Research is operated by the University Corporation for Atmospheric Research with funding from the National Science Foundation.

References

- Aghedo, A. M., Bowman, K. W., Worden, H. M., Kulawik, S. S., Shindell, D. T., Lamarque, J.-F., Faluvegi, G., Parrington, M., Jones, D. B. A., and Rast, S.: The vertical distribution of ozone instantaneous radiative forcing from satellite and chemistry climate models, *J. Geophys. Res.*, 116, D01305, doi:10.1029/2010JD014243, 2011.
- Barahona, D., West, R. E. L., Stier, P., Romakkaniemi, S., Kokkola, H., and Nenes, A.: Comprehensively accounting for the effect of giant CCN in cloud activation parameterizations, *Atmos. Chem. Phys.*, 10, 2467–2473, doi:10.5194/acp-10-2467-2010, 2010.
- Bennartz, R.: Global assessment of marine boundary layer cloud droplet number concentration from satellite, *J. Geophys. Res.*, 112, D02201, doi:10.1029/2006JD007547, 2007.
- Bond, T. C., Bhardwaj, E., Dong, R., Jogani, R., Jung, S., Roden, C., Streets, D. G., and Trautmann, N. M.: Historical emissions of black and organic carbon aerosol from energy-related combustion, 1850–2000, *Global Biogeochem. Cy.*, 21, GB2018, doi:10.1029/2006GB002840, 2007.
- Brock, C. A., Cozic, J., Bahreini, R., Froyd, K. D., Middlebrook, A. M., McComiskey, A., Brioude, J., Cooper, O. R., Stohl, A., Aikin, K. C., de Gouw, J. A., Fahey, D. W., Ferrare, R. A., Gao, R.-S., Gore, W., Holloway, J. S., Hübler, G., Jefferson, A., Lack, D. A., Lance, S., Moore, R. H., Murphy, D. M., Nenes, A., Novelli, P. C., Nowak, J. B., Ogren, J. A., Peischl, J., Pierce, R. B., Pilewskie, P., Quinn, P. K., Ryerson, T. B., Schmidt, K. S., Schwarz, J. P., Sodemann, H., Spackman, J. R., Stark, H., Thomson, D. S., Thornberry, T., Veres, P., Watts, L. A., Warneke, C., and Wollny, A. G.: Characteristics, sources, and transport of aerosols measured in spring 2008 during the aerosol, radiation, and cloud processes affecting Arctic Climate (ARCPAC) Project, *Atmos. Chem. Phys.*, 11, 2423–2453, doi:10.5194/acp-11-2423-2011, 2011.
- Cappa, C. D. and Jimenez, J. L.: Quantitative estimates of the volatility of ambient organic aerosol, *Atmos. Chem. Phys.*, 10, 5409–5424, doi:10.5194/acp-10-5409-2010, 2010.
- Chan, A. W. H., Kautzman, K. E., Chhabra, P. S., Surratt, J. D., Chan, M. N., Crounse, J. D., Kürten, A., Wennberg, P. O., Flagan, R. C., and Seinfeld, J. H.: Secondary organic aerosol

GMDD

8, 7189–7247, 2015

CESM/CAM5 improvement and application

J. He et al.

Title Page

Abstract

Introduction

Conclusions

References

Tables

Figures



Back

Close

Full Screen / Esc

Printer-friendly Version

Interactive Discussion



**CESM/CAM5
improvement and
application**

J. He et al.

Title Page

Abstract

Introduction

Conclusions

References

Tables

Figures



Back

Close

Full Screen / Esc

Printer-friendly Version

Interactive Discussion



formation from photooxidation of naphthalene and alkylnaphthalenes: implications for oxidation of intermediate volatility organic compounds (IVOCs), *Atmos. Chem. Phys.*, 9, 3049–3060, doi:10.5194/acp-9-3049-2009, 2009.

Couvidat, F., Kim, Y., Sartelet, K., Seigneur, C., Marchand, N., and Sciare, J.: Modeling secondary organic aerosol in an urban area: application to Paris, France, *Atmos. Chem. Phys.*, 13, 983–996, doi:10.5194/acp-13-983-2013, 2013.

Emmons, L. K., Walters, S., Hess, P. G., Lamarque, J.-F., Pfister, G. G., Fillmore, D., Granier, C., Guenther, A., Kinnison, D., Laepple, T., Orlando, J., Tie, X., Tyndall, G., Wiedinmyer, C., Baughcum, S. L., and Kloster, S.: Description and evaluation of the Model for Ozone and Related chemical Tracers, version 4 (MOZART-4), *Geosci. Model Dev.*, 3, 43–67, doi:10.5194/gmd-3-43-2010, 2010.

Fountoukis, C. and Nenes, A.: Continued development of a cloud droplet formation parameterization for global climate models, *J. Geophys. Res.*, 110, D11212, doi:10.1029/2004JD005591, 2005.

Fountoukis, C. and Nenes, A.: ISORROPIA II: a computationally efficient thermodynamic equilibrium model for $K^+ - Ca^{2+} - Mg^{2+} - NH_4^+ - Na^+ - SO_4^{2-} - NO_3^- - Cl^- - H_2O$ aerosols, *Atmos. Chem. Phys.*, 7, 4639–4659, doi:10.5194/acp-7-4639-2007, 2007.

Gantt, B., He, J., Zhang, X., Zhang, Y., and Nenes, A.: Incorporation of advanced aerosol activation treatments into CESM/CAM5: model evaluation and impacts on aerosol indirect effects, *Atmos. Chem. Phys.*, 14, 7485–7497, doi:10.5194/acp-14-7485-2014, 2014.

Gery, M. W., Whitten, G. Z., Killus, J. P., and Dodge, M. C.: A photochemical kinetics mechanism for urban and regional scale computer modeling, *J. Geophys. Res.*, 94, 12925–12956, doi:10.1029/JD094iD10p12925, 1989.

Glotfelty, T., He, J., and Zhang, Y.: Updated organic aerosol treatments in CESM/CAM5: development and initial application, in preparation, 2015.

Granier, C., Bessagnet, B., Bond, T., D'Angiola, A., Denier van der Gon, H., Frost, G. J., Heil, A., Kaiser, J. W., Kinne, S., Klimont, Z., Kloster, S., Lamarque, J.-F., Liousse, C., Masui, T., Meleux, F., Mieville, A., Ohara, T., Raut, J.-C., Riahi, K., Schultz, M. G., Smith, S. J., Thompson, A., van Aardenne, J., van der Werf, G. R., and van Vuuren, D. P.: Evolution of anthropogenic and biomass burning emissions of air pollutants at global and regional scales during the 1980–2010 period, *Climatic Change*, 109, 163–190, doi:10.1007/s10584-011-0154-1, 2011.

CESM/CAM5 improvement and application

J. He et al.

Title Page

Abstract

Introduction

Conclusions

References

Tables

Figures



Back

Close

Full Screen / Esc

Printer-friendly Version

Interactive Discussion



Guenther, A. B., Jiang, X., Heald, C. L., Sakulyanontvittaya, T., Duhl, T., Emmons, L. K., and Wang, X.: The Model of Emissions of Gases and Aerosols from Nature version 2.1 (MEGAN2.1): an extended and updated framework for modeling biogenic emissions, *Geosci. Model Dev.*, 5, 1471–1492, doi:10.5194/gmd-5-1471-2012, 2012.

5 He, J. and Zhang, Y.: Improvement and further development in CESM/CAM5: gas-phase chemistry and inorganic aerosol treatments, *Atmos. Chem. Phys.*, 14, 9171–9200, doi:10.5194/acp-14-9171-2014, 2014.

He, J., Zhang, Y., Glotfelty, T., He, R., Bennartz, R., Rausch, J., and Sartelet, K.: Decadal simulation and comprehensive evaluation of CESM/CAM5.1 and advanced chemistry, aerosol microphysics, and aerosol-cloud interactions, *J. Adv. Model. Earth Syst.*, 7, 110–141, doi:10.1002/2014MS000360, 2015.

10 Hodzic, A., Jimenez, J. L., Madronich, S., Canagaratna, M. R., DeCarlo, P. F., Kleinman, L., and Fast, J.: Modeling organic aerosols in a megacity: potential contribution of semi-volatile and intermediate volatility primary organic compounds to secondary organic aerosol formation, *Atmos. Chem. Phys.*, 10, 5491–5514, doi:10.5194/acp-10-5491-2010, 2010.

15 Jacob, D. J. and Winner, D. A.: Effect of climate change on air quality, *Atmos. Environ.*, 43, 51–63, 2009.

Jacob, D. J., Crawford, J. H., Maring, H., Clarke, A. D., Dibb, J. E., Emmons, L. K., Ferrare, R. A., Hostetler, C. A., Russell, P. B., Singh, H. B., Thompson, A. M., Shaw, G. E., McCauley, E., Pederson, J. R., and Fisher, J. A.: The Arctic Research of the Composition of the Troposphere from Aircraft and Satellites (ARCTAS) mission: design, execution, and first results, *Atmos. Chem. Phys.*, 10, 5191–5212, doi:10.5194/acp-10-5191-2010, 2010.

20 Jathar, S. H., Farina, S. C., Robinson, A. L., and Adams, P. J.: The influence of semi-volatile and reactive primary emissions on the abundance and properties of global organic aerosol, *Atmos. Chem. Phys.*, 11, 7727–7746, doi:10.5194/acp-11-7727-2011, 2011.

25 Jimenez, J. L., Canagaratna, M. R., Donahue, N. M., Prevot, A. S. H., Zhang, Q., Kroll, J. H., DeCarlo, P. F., Allan, J. D., Coe, H., Ng, N. L., Aiken, A. C., Docherty, K. S., Ulbrich, I. M., Grieshop, A. P., Robinson, A. L., Duplissy, J., Smith, J. D., Wilson, K. R., Lanz, V. A., Hueglin, C., Sunn, Y. L., Tian, J., Laaksonen, A., Raatikainen, T., Rautiainen, J., Vaatovaara, P., Ehn, M., Kulmala, M., Tomlinson, J. M., Collins, D. R., Cubison, M. J., Dunlea, E., J., Huffman, J. A., Onasch, T. B., Alfarra, M. R., Williams, P. I., Bower, K., Kondo, Y., Schneider, J., Drewnick, F., Borrmann, S., Weimer, S., Demerjian, K., Salcedo, D., Cottrell, L., Griffin, R., Takami, A., Miyoshi, T., Hatakeyama, S., Shimono, A., Sun, J. Y.,

CESM/CAM5 improvement and application

J. He et al.

Title Page

Abstract

Introduction

Conclusions

References

Tables

Figures



Back

Close

Full Screen / Esc

Printer-friendly Version

Interactive Discussion



Zhang, Y. M., Dzepina, K., Kimmel, J. R., Sueper, D., Jayne, J. T., Herndon, S. C., Trimborn, A. M., Williams, L. R., Wood, E. C., Middlebrook, A. M., Kolb, C. E., Baltensperger, U., and Worsnop, D. R.: Evolution of organic aerosols in the atmosphere, *Science*, 326, 1525–1529, doi:10.1126/science.1180353, 2009.

5 Karamchandani, P., Zhang, Y., Chen, S.-Y., and Balmori-Bronson, R.: Development of an extended chemical mechanism for global-through-urban applications, *Atmospheric Pollution Research*, 3, 1–24, 2012.

Kay, J. E., Hillman, B. R., Klein, S. A., Zhang, Y., Medeiros, B., Pincus, R., Gettelman, A., Eaton, B., Boyle, J., Marchand, R., and Ackerman, T. P.: Exposing global cloud biases in the Community Atmosphere Model (CAM) using satellite observations and their corresponding instrument simulators, *J. Climate*, 25, 5190–5207, doi:10.1175/JCLI-D-11-00469.1, 2012.

10 Kim, Y., Sartelet, K., and Seigneur, C.: Comparison of two gas-phase chemical kinetic mechanisms of ozone formation over Europe, *J. Atmos. Chem.*, 62, 89–119, doi:10.1007/s10874-009-9142-5, 2009.

15 Kim, Y., Sartelet, K., and Seigneur, C.: Formation of secondary aerosols over Europe: comparison of two gas-phase chemical mechanisms, *Atmos. Chem. Phys.*, 11, 583–598, doi:10.5194/acp-11-583-2011, 2011a.

Kim, Y., Couvidat, F., Sartelet, K., and Seigneur, C.: Comparison of different gas-phase mechanisms and aerosol modules for simulating particulate matter formation, *J. Air Waste Manage.*, 61, 1218–1226, doi:10.1080/10473289.2011.603999, 2011b.

20 Kinnison, D. E., Brasseur, G. P., Walters, S., Garcia, R. R., Marsh, D. A., Sassi, F., Boville, B. A., Harvey, L., Randall, C., Emmons, L., Lamarque, J.-F., Hess, P., Orlando, J., Tyndall, G., Tie, X. X., Randel, W., Pan, L., Gettelman, A., Granier, C., Diehl, T., Niemeier, U., and Simmons, A. J.: Sensitivity of chemical tracers to meteorological parameters in the MOZART-3 chemical transport model, *J. Geophys. Res.*, 112, D20302, doi:10.1029/2006JD007879, 2007.

25 Knote, C., Tuccella, P., Curci, G., Emmons, L., Orlando, J. J., Madronich, S., Baró, R., Jiménez-Guerrero, P., Luecken, D., Hogrefe, C., Forkel, R., Werhahn, J., Hirtl, M., Pérez, J. L., San José, R., Giordano, L., Brunner, D., Khairunnisa, Y., and Zhang, Y.: Influence of the choice of gas-phase mechanism on predictions of key gaseous pollutants during the AQMEII phase-2 intercomparison, *Atmos. Environ.*, 115, 553–568, doi:10.1016/j.atmosenv.2014.11.066, 2014a.

CESM/CAM5 improvement and application

J. He et al.

Title Page

Abstract

Introduction

Conclusions

References

Tables

Figures



Back

Close

Full Screen / Esc

Printer-friendly Version

Interactive Discussion



Knote, C., Hodzic, A., Jimenez, J. L., Volkamer, R., Orlando, J. J., Baidar, S., Brioude, J., Fast, J., Gentner, D. R., Goldstein, A. H., Hayes, P. L., Knighton, W. B., Oetjen, H., Setyan, A., Stark, H., Thalman, R., Tyndall, G., Washenfelder, R., Waxman, E., and Zhang, Q.: Simulation of semi-explicit mechanisms of SOA formation from glyoxal in aerosol in a 3-D model, *Atmos. Chem. Phys.*, 14, 6213–6239, doi:10.5194/acp-14-6213-2014, 2014b.

Kumar, P., Sokolik, I. N., and Nenes, A.: Parameterization of cloud droplet formation for global and regional models: including adsorption activation from insoluble CCN, *Atmos. Chem. Phys.*, 9, 2517–2532, doi:10.5194/acp-9-2517-2009, 2009.

Lamarque, J.-F. and Solomon, S.: Impact of changes in climate and halocarbons on recent lower stratosphere ozone and temperature trends, *J. Climate*, 23, 2599–2611, 2010.

Lamarque, J.-F., Kinnison, D. E., Hess, P. G., and Vitt, F.: Simulated lower stratospheric trends between 1970 and 2005: identifying the role of climate and composition changes, *J. Geophys. Res.*, 113, D12301, doi:10.1029/2007JD009277, 2008.

Lamarque, J.-F., Bond, T. C., Eyring, V., Granier, C., Heil, A., Klimont, Z., Lee, D., Liousse, C., Mieville, A., Owen, B., Schultz, M. G., Shindell, D., Smith, S. J., Stehfest, E., Van Aardenne, J., Cooper, O. R., Kainuma, M., Mahowald, N., McConnell, J. R., Naik, V., Riahi, K., and van Vuuren, D. P.: Historical (1850–2000) gridded anthropogenic and biomass burning emissions of reactive gases and aerosols: methodology and application, *Atmos. Chem. Phys.*, 10, 7017–7039, doi:10.5194/acp-10-7017-2010, 2010.

Lamarque, J.-F., McConnell, J. R., Shindell, D. T., Orlando, J. J., and Tyndall, G. S.: Understanding the drivers for the 20th century change of hydrogen peroxide in Antarctic ice-cores, *Geophys. Res. Lett.*, 38, L04810, doi:10.1029/2010GL045992, 2011a.

Lamarque, J.-F., Kyle, G. P., Meinshausen, M., Riahi, K., Smith, S. J., van Vuuren, D. P., Conley, A., and Vitt, F.: Global and regional evolution of short-lived radiatively-active gases and aerosols in the Representative Concentration Pathways, *Climatic Change*, 109, 191–212, 2011b.

Lamarque, J.-F., Emmons, L. K., Hess, P. G., Kinnison, D. E., Tilmes, S., Vitt, F., Heald, C. L., Holland, E. A., Lauritzen, P. H., Neu, J., Orlando, J. J., Rasch, P. J., and Tyndall, G. K.: CAM-chem: description and evaluation of interactive atmospheric chemistry in the Community Earth System Model, *Geosci. Model Dev.*, 5, 369–411, doi:10.5194/gmd-5-369-2012, 2012.

Lamarque, J.-F., Shindell, D. T., Josse, B., Young, P. J., Cionni, I., Eyring, V., Bergmann, D., Cameron-Smith, P., Collins, W. J., Doherty, R., Dalsoren, S., Faluvegi, G., Folberth, G., Ghan, S. J., Horowitz, L. W., Lee, Y. H., MacKenzie, I. A., Nagashima, T., Naik, V., Plum-

CESM/CAM5 improvement and application

J. He et al.

Title Page

Abstract

Introduction

Conclusions

References

Tables

Figures



Back

Close

Full Screen / Esc

Printer-friendly Version

Interactive Discussion



mer, D., Righi, M., Rumbold, S. T., Schulz, M., Skeie, R. B., Stevenson, D. S., Strode, S., Sudo, K., Szopa, S., Voulgarakis, A., and Zeng, G.: The Atmospheric Chemistry and Climate Model Intercomparison Project (ACCMIP): overview and description of models, simulations and climate diagnostics, *Geosci. Model Dev.*, 6, 179–206, doi:10.5194/gmd-6-179-2013, 2013.

Levy, R. C., Mattoo, S., Munchak, L. A., Remer, L. A., Sayer, A. M., Patadia, F., and Hsu, N. C.: The Collection 6 MODIS aerosol products over land and ocean, *Atmos. Meas. Tech.*, 6, 2989–3034, doi:10.5194/amt-6-2989-2013, 2013.

Lewandowski, M., Piletic, I. R., Kleindienst, T. E., Offenberg, J. H., Beaver, M. R., Jaoui, M., Docherty, K. S., and Edney, E. O.: Secondary organic aerosol characterization at field sites across the United States during the spring-summer period, *Int. J. Environ. An. Ch.*, 93, 1084–1103, 2013.

Liu, X., Easter, R. C., Ghan, S. J., Zaveri, R., Rasch, P., Shi, X., Lamarque, J.-F., Gettelman, A., Morrison, H., Vitt, F., Conley, A., Park, S., Neale, R., Hannay, C., Ekman, A. M. L., Hess, P., Mahowald, N., Collins, W., Iacono, M. J., Bretherton, C. S., Flanner, M. G., and Mitchell, D.: Toward a minimal representation of aerosols in climate models: description and evaluation in the Community Atmosphere Model CAM5, *Geosci. Model Dev.*, 5, 709–739, doi:10.5194/gmd-5-709-2012, 2012.

Luecken, D. J., Phillips, S., Sarwar, G., and Jang, C.: Effects of using the CB05 vs. SAPRC99 vs. CB4 chemical mechanism on model predictions: ozone and gas-phase photochemical precursor concentrations, *Atmos. Environ.*, 42, 5805–5820, doi:10.1016/j.atmosenv.2007.08.056, 2008.

Ma, P.-L., Rasch, P. J., Wang, H., Zhang, K., Easter, R. C., Tilmes, S., Fast, J. D., Liu, X., Yoon, J.-H., and Lamarque, J.-F.: The role of circulation features on black carbon transport into the Arctic in the Community Atmosphere Model version 5 (CAM5), *J. Geophys. Res.-Atmos.*, 118, 4657–4669, doi:10.1002/jgrd.50411, 2013.

Martensson, E. M., Nilsson, E. D., deLeeuw, G., Cohen, L. H., and Hansson, H. C.: Laboratory simulations and parameterization of the primary marine aerosol production, *J. Geophys. Res.*, 108, 4297, doi:10.1029/2002JD002263, 2003.

May, A. A., Presto, A. A., Hennigan, C. J., Nguyen, N. T., Gordon, T. D., and Robinson, A. I.: Gas-particle partitioning of primary organic aerosol emissions: (1), gasoline vehicle exhaust, *Atmos. Environ.*, 77, 128–139, doi:10.1016/j.atmosenv.2013.04.060, 2013a.

CESM/CAM5 improvement and application

J. He et al.

Title Page

Abstract

Introduction

Conclusions

References

Tables

Figures



Back

Close

Full Screen / Esc

Printer-friendly Version

Interactive Discussion



May, A. A., Levin, E. J. T., Hennigan, C. J., Riipinen, I., Lee, T., Collett Jr., J. L., Jimenez, J. L., Kreidenweis, S. M., and Robinson, A. L.: Gas-particle partitioning of primary organic aerosol emissions: 3. Biomass burning, *J. Geophys. Res.-Atmos.*, 118, 11,327–11,338, doi:10.1002/jgrd.50828, 2013b.

5 Merikanto, J., Napari, I., Vehkamäki, H., Anttila, T., and Kulmala, M.: New parameterization of sulfuric acid-ammonia-water ternary nucleation rates at tropospheric conditions, *J. Geophys. Res.*, 112, D15207, doi:10.1029/2006JD007977, 2007.

Pan, L. L., Bowman, K. P., Atlas, E. L., Wofsy, S. C., Zhang, F., Bresch, J. F., Ridley, B. A., Pittman, J. V., Homeyer, C. R., Romashkin, P., and Cooper, W. A.: The stratosphere–troposphere analyses of regional transport 2008 (START08) experiment, *B. Am. Meteorol. Soc.*, 91, 327–342, 2010.

Price, C. and Rind, D.: A simple lightning parameterization for calculating global lightning distributions, *J. Geophys. Res.*, 97, 9919–9933, doi:10.1029/92JD00719, 1992.

Price, C., Penner, J., and Prather, M.: NO_x from lightning 1, Global distribution based on lightning physics, *J. Geophys. Res.*, 102, 5929–5941, 1997.

15 Reutter, P., Su, H., Trentmann, J., Simmel, M., Rose, D., Gunthe, S. S., Wernli, H., Andreae, M. O., and Pöschl, U.: Aerosol- and updraft-limited regimes of cloud droplet formation: influence of particle number, size and hygroscopicity on the activation of cloud condensation nuclei (CCN), *Atmos. Chem. Phys.*, 9, 7067–7080, doi:10.5194/acp-9-7067-2009, 2009.

20 Robinson, A. L., Donahue, N. M., Shrivastava, M. K., Weitkamp, E. A., Sage, A. M., Grieshop, A. P., Lane, T. E., Pierce, J. R., and Pandis, S. N.: Rethinking organic aerosols: semivolatile emissions and photochemical aging, *Science*, 315, 1259–1262, doi:10.1126/science.1133061, 2007.

25 Ryerson, T. B., Andrews, A. E., Angevine, W. M., Bates, T. S., Brock, C. A., Cairns, B., Cohen, R. C., Cooper, O. R., de Gouw, J. A., Fehsenfeld, F. C., Ferrare, R. A., Fischer, M. L., Flagan, R. C., Goldstein, A. H., Hair, J. W., Hardesty, R. M., Hostetler, C. A., Jimenez, J. L., Langford, A. O., McCauley, E., McKeen, S. A., Molina, L. T., Nenes, A., Oltmans, S. J., Parrish, D. D., Pederson, J. R., Pierce, R. B., Prather, K., Quinn, P. K., Seinfeld, J. H., Senff, C. J., Sorooshian, A., Stutz, J., Surratt, J. D., Trainer, M., Volkamer, R., Williams, E. J., and Wofsy, S. C.: The 2010 California Research at the Nexus of Air Quality and Climate Change (CalNex) field study, *J. Geophys. Res.*, 118, 5830–5866, doi:10.1002/jgrd.50331, 2013.

CESM/CAM5 improvement and application

J. He et al.

Title Page

Abstract

Introduction

Conclusions

References

Tables

Figures



Back

Close

Full Screen / Esc

Printer-friendly Version

Interactive Discussion



Sarwar, G., Luecken, D., Yarwood, G., Whitten, G., and Carter, W. P. L.: Impact of an updated carbon bond mechanism on predictions from the Community Multiscale Air Quality Model, *J. Appl. Meteorol. Clim.*, 47, 3–14, doi:10.1175/2007JAMC1393.1, 2008.

Seethala, C. and Horvath, Á.: Global assessment of AMSR-E and MODIS cloud liquid water path retrievals in warm oceanic clouds, *J. Geophys. Res.*, 115, D13202, doi:10.1029/2009JD012662, 2010.

Shrivastava, M. K., Lane, T. E., Donahue, N. M., Pandis, S. N., and Robinson, A. L.: Effects of gas particle partitioning and aging of primary emissions on urban and regional organic aerosol concentrations, *J. Geophys. Res.*, 113, D18301, doi:10.1029/2007JD009735, 2008.

Shrivastava, M., Zelenyuk, A., Imre, D., Easter, R., Beranek, J., Zaveri, R. A., and Fast, J.: Implications of low volatility SOA and gas-phase fragmentation reactions on SOA loadings and their spatial and temporal evolution in the atmosphere, *J. Geophys. Res.*, 118, 3328–3342, doi:10.1002/jgrd.50160, 2013.

Smith, S. J., van Aardenne, J., Klimont, Z., Andres, R. J., Volke, A., and Delgado Arias, S.: Anthropogenic sulfur dioxide emissions: 1850–2005, *Atmos. Chem. Phys.*, 11, 1101–1116, doi:10.5194/acp-11-1101-2011, 2011.

Stainer, C. O., Donahue, N., and Pandis, S. N.: Parameterization of secondary organic aerosol mass fractions from smog chamber data, *Atmos. Environ.*, 42, 2276–2299, doi:10.1016/j.atmosenv.2007.12.042, 2008.

Taylor, K. E.: Summarizing multiple aspects of model performance in a single diagram, *J. Geophys. Res.*, 106, 7183–7192, 2001.

Tilmes, S., Lamarque, J.-F., Emmons, L. K., Kinnison, D. E., Ma, P.-L., Liu, X., Ghan, S., Bardeen, C., Arnold, S., Deeter, M., Vitt, F., Ryerson, T., Elkins, J. W., Moore, F., Spackman, J. R., and Val Martin, M.: Description and evaluation of tropospheric chemistry and aerosols in the Community Earth System Model (CESM1.2), *Geosci. Model Dev.*, 8, 1395–1426, doi:10.5194/gmd-8-1395-2015, 2015.

Tsimpidi, A. P., Karydis, V. A., Zavala, M., Lei, W., Molina, L., Ulbrich, I. M., Jimenez, J. L., and Pandis, S. N.: Evaluation of the volatility basis-set approach for the simulation of organic aerosol formation in the Mexico City metropolitan area, *Atmos. Chem. Phys.*, 10, 525–546, doi:10.5194/acp-10-525-2010, 2010.

Vehkamäki, H., Kulmala, M., Napari, I., Lehtinen, K. E. J., Timmreck, C., Noppel, M., and Laaksonen, A.: An improved parameterization for sulfuric acid-water nucleation

CESM/CAM5 improvement and application

J. He et al.

Title Page

Abstract

Introduction

Conclusions

References

Tables

Figures



Back

Close

Full Screen / Esc

Printer-friendly Version

Interactive Discussion



rates for tropospheric and stratospheric conditions, *J. Geophys. Res.-Atmos.*, 107, 4622, doi:10.1029/2002JD002184, 2002.

Wang, H., Easter, R. C., Rasch, P. J., Wang, M., Liu, X., Ghan, S. J., Qian, Y., Yoon, J.-H., Ma, P.-L., and Vinoj, V.: Sensitivity of remote aerosol distributions to representation of cloud–aerosol interactions in a global climate model, *Geosci. Model Dev.*, 6, 765–782, doi:10.5194/gmd-6-765-2013, 2013.

Wang, K., Yahya, K., Zhang, Y., Wu, S.-Y., and Grell, G.: Implementation and initial application of a new chemistry-aerosol option in WRF/Chem for simulation secondary organic aerosols and aerosol indirect effects, *Atmos. Environ.*, 115, 716–732, doi:10.1016/j.atmosenv.2014.12.007, 2014.

Wang, M. and Penner, J. E.: Aerosol indirect forcing in a global model with particle nucleation, *Atmos. Chem. Phys.*, 9, 239–260, doi:10.5194/acp-9-239-2009, 2009.

Washenfelder, R., Young, C., Brown, S., Angevine, W., Atlas, E., Blake, D., Bon, D., Cubison, M., De Gouw, J., Dusanter, S., Flynn, J., Gilman, J. B., Graus, M., Griffith, S., Grossberg, N., Hayes, P. L., Jimenez, J., Kuster, W., Lefer, B. L., Pollack, I., Ryerson, T., Stark, H., Stevens, P. S., and Trainer, M.: The glyoxal budget and its contribution to organic aerosol for Los Angeles, California, during CalNex 2010, *J. Geophys. Res.*, 116, D00V02, doi:10.1029/2011JD016314, 2011.

Young, P. J., Archibald, A. T., Bowman, K. W., Lamarque, J.-F., Naik, V., Stevenson, D. S., Tilmes, S., Voulgarakis, A., Wild, O., Bergmann, D., Cameron-Smith, P., Cionni, I., Collins, W. J., Dalsøren, S. B., Doherty, R. M., Eyring, V., Faluvegi, G., Horowitz, L. W., Josse, B., Lee, Y. H., MacKenzie, I. A., Nagashima, T., Plummer, D. A., Righi, M., Rumbold, S. T., Skeie, R. B., Shindell, D. T., Strode, S. A., Sudo, K., Szopa, S., and Zeng, G.: Pre-industrial to end 21st century projections of tropospheric ozone from the Atmospheric Chemistry and Climate Model Intercomparison Project (ACCMIP), *Atmos. Chem. Phys.*, 13, 2063–2090, doi:10.5194/acp-13-2063-2013, 2013.

Yarwood, G., Rao, S., Yocke, M., and Whitten, G. Z.: Updates to the Carbon Bond Mechanism: CB05, Report to the U.S. Environmental Protection Agency, RT-04–00675, 2005.

Yu, F.: Ion-mediated nucleation in the atmosphere: key controlling parameters, implications, and look-up table, *J. Geophys. Res.*, 115, D03206, doi:10.1029/2009JD012630, 2010.

Zender, C. S., Bian, H., and Newman, D.: The mineral Dust Entrainment And Deposition (DEAD) model: description and 1990s dust climatology, *J. Geophys. Res.*, 108, 4416, doi:10.1029/2002JD002775, 2003.

CESM/CAM5 improvement and application

J. He et al.

Title Page

Abstract

Introduction

Conclusions

References

Tables

Figures



Back

Close

Full Screen / Esc

Printer-friendly Version

Interactive Discussion



Zhang, Q., Jimenez, J. L., Canagaratna, M. R., Allan, J. D., Coe, H., Ulbrich, I., Alfarra, M. R., Takami, A., Middlebrook, A. M., Sun, Y. L., Dzepina, K., Dunlea, E., Docherty, K., DeCarlo, P. F., Salcedo, D., Onasch, T., Jayne, J. T., Miyoshi, T., Shimo, A., Hatakeyama, S., Takegawa, N., Kondo, Y., Schneider, J., Drewnick, F., Borrmann, S., Weimer, S., Demerjian, K., Williams, P., Bower, K., Bahreini, R., Cottrell, L., Griffin, R. J., Rautiainen, J., Sun, J. Y., Zhang, Y. M., and Worsnop, D. R.: Ubiquity and dominance of oxygenated species in organic aerosols in anthropogenically-influenced Northern Hemisphere midlatitudes, *Geophys. Res. Lett.*, 34, L13801, doi:10.1029/2007GL029979, 2007.

Zhang, Q., Quan, J., Tie, X., Huang, M., and Ma, X.: Impacts of aerosol particles on cloud formation: aircraft measurements in China, *Atmos. Environ.*, 45, 665–672, 2011.

Zhang, Y., Pun, B., Vijayaraghavan, K., Wu, S.-Y., Seigneur, C., Pandis, S., Jacobson, M., Nenes, A., and Seinfeld, J. H.: Development and application of the Model of Aerosol Dynamics, Reaction, Ionization and Dissolution (MADRID), *J. Geophys. Res.*, 109, D01202, doi:10.1029/2003JD003501, 2004.

Zhang, Y., Karamchandani, P., Glotfelty, T., Street, D. G., Grell, G., Nenes, A., Yu, F., and Benartz, R.: Development and initial application of the global-through-urban weather research and forecasting model with chemistry (GU-WRF/Chem), *J. Geophys. Res.*, 117, D20206, doi:10.1029/2012JD017966, 2012a.

Zhang, Y., Chen, Y., Sarwar, G., and Schere, K.: Impacts of gas-phase mechanisms on weather research forecasting model with chemistry (WRF/Chem) predictions: mechanism implementation and comparative evaluation, *J. Geophys. Res.*, 117, D01301, doi:10.1029/2011JD015775, 2012b.

Zhang, Y., Zhang, X., Wang, L.-T., Zhang, Q., Duan, F.-K., and He, K.-B.: Application of WRF/Chem over East Asia: Part I. Model evaluation and intercomparison with MM5/CMAQ, *Atmos. Environ.*, doi:10.1016/j.atmosenv.2015.07.023, in press, 2015a.

Zhang, Y., Zhang, X., Wang, K., Zhang, Q., Duan, F.-K., and He, K.-B.: Application of WRF/Chem over East Asia: Part II. Model improvement and sensitivity simulations, *Atmos. Environ.*, doi:10.1016/j.atmosenv.2015.07.022, in press, 2015b.

CESM/CAM5
improvement and
application

J. He et al.

Title Page

Abstract

Introduction

Conclusions

References

Tables

Figures



Back

Close

Full Screen / Esc

Printer-friendly Version

Interactive Discussion

**Table 1.** Gas-phase organic aerosol precursors in the two mechanisms.

Precursors	MOZART-4x ^a	CB05_GE ^b
Aromatics	TOLUENE, BENZENE, XYLENES, CRESOL	TOL, XYL, CRES, PAH
Alkanes	BIGALK	ALKH
Anthropogenic alkenes	C3H6, BIGENE	OLE, IOLE
Biogenic alkenes	APIN, BPIN, LIMON, MYRC, BCARY, ISOP	APIN, BPIN, LIM, OCI, HUM, TER, ISOP

^a BIGALK: lumped alkanes C > 3; C₃H₆: propene; BIGENE: lumped alkenes C > 3; APIN: α -pinene + others; BPIN: β -pinene + others; LIMON: limonene + others; MYRC: myrcene + others; BCARY: beta-caryophyllene + other sesquiterpenes; ISOP: isoprene.

^b TOL: toluene and other monoalkyl aromatics; XYL: xylene and other polyalkyl aromatics; CRES: cresol and higher molecular weight phenols; PAH: polycyclic aromatic hydrocarbons; ALKH: long-chain alkanes, C > 6; OLE: terminal olefin carbon bond (R-C = C); IOLE: internal olefin carbon bond (R-C = C-R); APIN: α -pinene; BPIN: β -pinene; LIM: limonene; OCI: ocimene; HUM: humulene; TER: terpinene; ISOP: isoprene.

Table 2. Continued.

Species/Variables	Dataset (Number of sites)
Chloride (Cl ⁻)	CONUS: IMPROVE (199) Europe: Airbase (3846), EMEP (317)
Organic carbon (OC)	CONUS: IMPROVE (199); Europe: EMEP (317)
Black carbon (BC), Total carbon (TC)	CONUS: IMPROVE (199), STN(18 129)
Formaldehyde (HCHO), Isoprene (ISOP), and Toluene (TOL)	CONUS: AQS (25 877)
Hydrocarbon-like organic aerosol (HOA), Oxygenated organic aerosol (OOA), Total organic aerosol (TOA)	Northern Hemisphere: Zhang et al. (2007) and Jimenez et al. (2009) (Z07 and J09) (33)
Secondary organic aerosol (SOA)	CONUS: Ohio (2) and California (2) (Lewandowski et al., 2013)
Particulate matter with diameter less than and equal to 2.5 µm (PM _{2.5})	CONUS: IMPROVE (199), STN (18 129) Europe: BDQA (490), EMEP (317)
Particulate matter with diameter less than and equal to 10 µm (PM ₁₀)	CONUS: AQS (25 877) Europe: Airbase (3846), BDQA (490), EMEP (317) East Asia: MEPC (84), NIESJ (2133), KMOE (258), TAQMN (70)
Column CO	Globe: MOPITT
Column NO ₂ , Column SO ₂ , Column HCHO, Column glyoxal (C ₂ H ₂ O ₂)	Globe: SCIAMACHY
Tropospheric ozone residual (TOR)	Globe: OMI/MLS
O ₃ , CO, NO _x , and NO _y profiles	ARCPAC (Mar–Apr 2008), ARCTAS (Apr–Jun 2008), START08 (Apr–Jun 2008), and CalNex (May–Jun 2010)
CCN_China	Beijing: Zhang et al. (2011) (Jul–Sep 2008)

NOAA/CDC: National Oceanic and Atmospheric Administration Climate Diagnostics Center; MODIS: Moderate Resolution Imaging Spectroradiometer; CERES: Clouds and Earth's Radiant Energy System; MOPITT: the Measurements Of Pollution In The Troposphere; OMI/MLS: the Aura Ozone Monitoring Instrument in combination with Aura Microwave Limb Sounder; SCIAMACHY: the SCanning Imaging Absorption spectrometer for Atmospheric CHartography; CASTNET: Clean Air Status and Trends Network; IMPROVE: Interagency Monitoring of Protected Visual Environments; STN: Speciation Trends Network; AQS: Air Quality System; EMEP: European Monitoring and Evaluation Program; BDQA: Base de Données sur la Qualité de l'Air; AirBase: European air quality database; MEPC: Ministry of Environmental Protection of China; TAQMN: Taiwan Air Quality Monitoring Network; NIESJ: National Institute for Environmental Studies of Japan; KMOE: Korean Ministry of Environment; ARCPAC: Aerosol, Radiation, and Cloud Processes affecting Arctic Climate in 2008 (Brook et al., 2011); ARCTAS: Arctic Research of the Composition of the Troposphere from Aircraft and Satellites (Jacob et al., 2010), START08: Stratosphere–Troposphere Analyses of Regional Transport in 2008 (Pan et al., 2010); CalNex: California Nexus 2010 (Ryerson et al., 2013).

GMDD

8, 7189–7247, 2015

CESM/CAM5 improvement and application

J. He et al.

Title Page

Abstract

Introduction

Conclusions

References

Tables

Figures

◀

▶

◀

▶

Back

Close

Full Screen / Esc

Printer-friendly Version

Interactive Discussion



Table 3. Performance statistics of chemical species.

Species	Domain	Obs	MOZART-4x			CB05_GE		
			Sim	NMB (%) ^f	NME (%) ^f	Sim	NMB (%) ^f	NME (%) ^f
CO (ppb)	East Asia	438.7	150.9	-65.6	65.7	150.4	-65.7	65.8
SO ₂ ^a	CONUS	1.7	11.6	580.2	580.2	11.2	561.6	561.6
	Europe	4.7	9.5	100.9	121.2	9.2	94.1	115.4
	East Asia	2.9	4.3	47.0	70.6	3.9	35.5	64.0
NH ₃ ($\mu\text{g m}^{-3}$)	Europe	1.2	2.5	112.4	146.0	2.4	104.3	139.8
NO ₂ ^b	Europe	17.4	6.7	-61.4	65.5	6.6	-62.1	66.0
	East Asia	11.7	3.0	-74.1	75.2	3.0	-74.8	75.8
O ₃ ^c	CONUS	34.7	44.7	29.0	29.5	44.4	28.2	28.5
	Europe	56.2	78.6	39.9	40.8	80.6	43.5	44.2
	East Asia	29.8	48.3	62.4	62.4	47.7	60.3	60.3
HNO ₃ ($\mu\text{g m}^{-3}$)	CONUS	0.9	2.1	145.0	145.2	2.2	154.7	154.7
	Europe	0.8	0.7	-15.6	65.4	0.8	-10.9	64.9
HCHO (ppb)	CONUS	2.3	1.6	-30.1	48.4	1.5	-36.3	49.0
ISOP (ppb)	CONUS	0.3	0.2	-27.3	63.2	0.2	-29.0	64.7
Toluene (ppb)	CONUS	0.5	0.2	-65.3	69.2	0.2	-65.1	69.1
Col. CO (moleccm ⁻²)	Globe	1.6×10^{18}	1.2×10^{18}	-25.8	27.5	1.2×10^{18}	-24.4	26.1
Col. NO ₂ (moleccm ⁻²)	Globe	5.5×10^{14}	8.5×10^{14}	56.0	71.0	9.3×10^{14}	70.2	83.3
Col. HCHO (moleccm ⁻²)	Globe	4.6×10^{15}	3.1×10^{15}	-31.2	39.2	3.1×10^{15}	-32.7	40.4
Col. C ₂ H ₂ O ₂ (moleccm ⁻²)	Globe	2.8×10^{14}	3.9×10^{13}	-86.0	86.0	5.9×10^{12}	-97.9	-97.9
Col. SO ₂ (DU)	Globe	1.2	0.3	-70.1	90.1	0.3	-73.5	88.7

Title Page

Abstract

Introduction

Conclusions

References

Tables

Figures



Back

Close

Full Screen / Esc

Printer-friendly Version

Interactive Discussion



Table 3. Continued.

Species	Domain	Obs	MOZART-4x			CB05_GE		
			Sim	NMB (%) ^f	NME (%) ^f	Sim	NMB (%) ^f	NME (%) ^f
TOR (DU)	Globe	28.6	30.3	6.0	15.0	31.8	11.3	16.5
SO ₄ ²⁻ (µg m ⁻³)	CONUS	1.8	3.0	72.9	72.9	3.3	89.7	89.7
	Europe	1.8	2.9	62.1	70.1	3.2	79.7	85.2
NH ₄ ⁺ (µg m ⁻³)	CONUS	0.9	1.3	37.8	49.9	1.3	44.3	55.6
	Europe	0.9	1.3	51.5	63.1	1.4	63.4	72.8
NO ₃ ⁻ (µg m ⁻³)	CONUS	0.9	0.9	-6.0	44.4	0.7	-21.2	40.2
	Europe	1.7	1.2	-28.9	54.2	1.2	-30.5	53.4
Cl ⁻ (µg m ⁻³)	CONUS	0.1	0.02	-78.1	84.3	0.02	-78.3	84.5
	Europe	1.1	4.1	273.4	274.7	4.2	273.7	274.8
BC (µg m ⁻³)	CONUS	0.3	0.2	-29.3	44.6	0.2	-29.3	44.6
OC (µg m ⁻³)	CONUS	0.9	1.0	2.1	33.2	0.7	-20.7	32.8
	Europe	2.9	0.7	-74.2	77.3	0.7	-75.1	78.0
TC (µg m ⁻³)	CONUS	1.8	1.3	-29.6	39.3	1.1	-42.1	45.8
SOA ^d	CONUS	1.8	1.8	-1.9	29.3	1.4	-23.1	35.8
HOA ^d	N.H. ^e	2.1	0.5	-77.2	81.5	0.5	-76.7	81.3
OOA ^d	N.H. ^e	4.8	2.1	-56.5	56.6	1.8	-62.3	62.3
TOA ^d	N.H. ^e	7.9	2.5	-67.8	68.2	2.3	-71.2	72.0
PM _{2.5} (µg m ⁻³)	CONUS	7.4	7.5	0.7	27.6	7.4	-1.1	27.7
	Europe	14.4	8.9	-39.8	44.8	9.0	-37.4	42.9
PM ₁₀ (µg m ⁻³)	CONUS	20.6	12.6	-38.6	50.2	12.6	-38.9	50.7
	Europe	22.1	18.8	-14.9	39.9	19.2	-13.1	38.9
	East Asia	88.0	59.0	-32.9	41.1	64.8	-26.4	37.2

^a The unit is µg m⁻³ for CONUS and ppb for East Asia. ^b The unit is µg m⁻³ for Europe and ppb for East Asia. ^c The unit is ppb for CONUS and East Asia, and µg m⁻³ for Europe. ^d SOA: secondary organic aerosol; HOA: hydrocarbon-like organic aerosol; OOA: oxygenated organic aerosol; TOA: total organic aerosol; ^e N.H.: Northern Hemisphere; ^f MB: mean bias; NMB: normalized mean bias (%); NME: normalized mean error (%); RMSE: root mean squared error; Corr.: correlation coefficient.

Title Page

Abstract

Introduction

Conclusions

References

Tables

Figures



Back

Close

Full Screen / Esc

Printer-friendly Version

Interactive Discussion



CESM/CAM5 improvement and application

J. He et al.

Table 4. Tropospheric Ozone Budget.

Ozone	MOZART-4x	CB05_GE	Lamarque et al. (2012)	Young et al. (2013)
Burden (Tg)	325	333	328	337 ± 23
Dry Deposition (Tgyr ⁻¹)	679	705	705	1003 ± 200
^a Chemical Production (Tgyr ⁻¹)	4974	5743	4897	5110 ± 606
^b Chemical Loss (Tgyr ⁻¹)	4259	5194	4604	4668 ± 727
Lifetime (days)	24	21	26	22.3 ± 2.0

^a Chemical production is mainly contributed by reactions of NO with peroxy radicals;

^b Chemical loss is mainly contributed by the oxygen radical in the O(¹D) + water (H₂O) reaction and by the reactions of ozone with the hydroperoxyl radical (HO₂), OH, and alkenes.

[Title Page](#)
[Abstract](#)
[Introduction](#)
[Conclusions](#)
[References](#)
[Tables](#)
[Figures](#)
[Back](#)
[Close](#)
[Full Screen / Esc](#)
[Printer-friendly Version](#)
[Interactive Discussion](#)


CESM/CAM5
improvement and
application

J. He et al.

Table 5. Performance statistics of meteorological/radiative variables.

Variables ^a	Networks	Obs	MOZART-4x				CB05_GE					
			Sim	NMB (%) ^b	NME (%) ^b	RMSE ^b	Corr ^b	Sim	NMB (%) ^b	NME (%) ^b	RMSE ^b	Corr ^b
OLR (Wm^{-2})	NOAA/CDC	217.0	224.8	3.6	4.1	10.0	0.99	223.7	3.1	3.9	9.6	0.98
FLDS (Wm^{-2})	CERES	306.7	307.3	0.2	3.1	11.6	0.99	307.3	0.2	3.1	11.5	0.99
FSDS (Wm^{-2})	CERES	163.4	150.9	-7.6	10.2	22.6	0.9	150.8	-7.7	10.2	22.7	0.9
SWCF (Wm^{-2})	CERES	-40.7	-51.5	26.4	33.4	19.0	0.9	-52.0	27.7	-34.4	19.6	0.9
LWCF (Wm^{-2})	CERES	22.4	17.6	-21.6	25.1	6.8	0.9	18.7	-16.7	23.8	6.6	0.9
CCN5 ($\# cm^{-2}$)	MODIS	2.2×10^8	1.5×10^8	-32.1	46.4	1.7×10^8	0.4	1.6×10^8	-29.0	46.6	1.7×10^8	0.4
CF (%)	MODIS	67.3	71.5	6.3	12.7	12.5	0.8	71.3	6.0	12.7	12.5	0.8
COT	MODIS	16.5	12.2	-26.0	61.6	14.0	-0.3	12.2	-26.0	61.3	14.0	-0.3
AOD	MODIS	0.15	0.11	-23.9	40.5	0.08	0.7	0.11	-24.6	40.5	0.08	0.7
PWV (cm)	MODIS	1.9	2.0	5.6	11.4	0.3	0.99	2.0	5.5	11.4	0.3	0.99
CDNC ($\# cm^{-3}$)	UM-W	105.8	126.6	19.7	38.7	56.5	0.5	127.8	20.8	39.1	58.1	0.6
LWP ($g m^{-2}$)	MODIS	142.0	65.2	-54.1	65.4	143.3	-0.4	64.7	-54.4	65.3	143.3	-0.4
	UM-W	84.6	87.0	2.8	38.3	42.3	0.4	86.0	1.7	37.7	41.7	0.4

^a OLR: outgoing long wave radiation; FLDS: downwelling longwave radiation at the surface; FSDS: downwelling shortwave radiation at the surface; SWCF: shortwave cloud radiative forcing; LWCF: longwave cloud radiative forcing; CCN5: column CCN (ocean) at supersaturation of 0.5%; CF: cloud fraction; COT: clout optical thickness; AOD: aerosol optical depth; PWV: precipitable water vapor; CDNC: cloud droplet number concentration; LWP: liquid water path.

^b NMB: normalized mean bias (%); NME: normalized mean error (%); RMSE: root mean squared error; Corr.: correlation coefficient.

Title Page

Abstract

Introduction

Conclusions

References

Tables

Figures

◀

▶

◀

▶

Back

Close

Full Screen / Esc

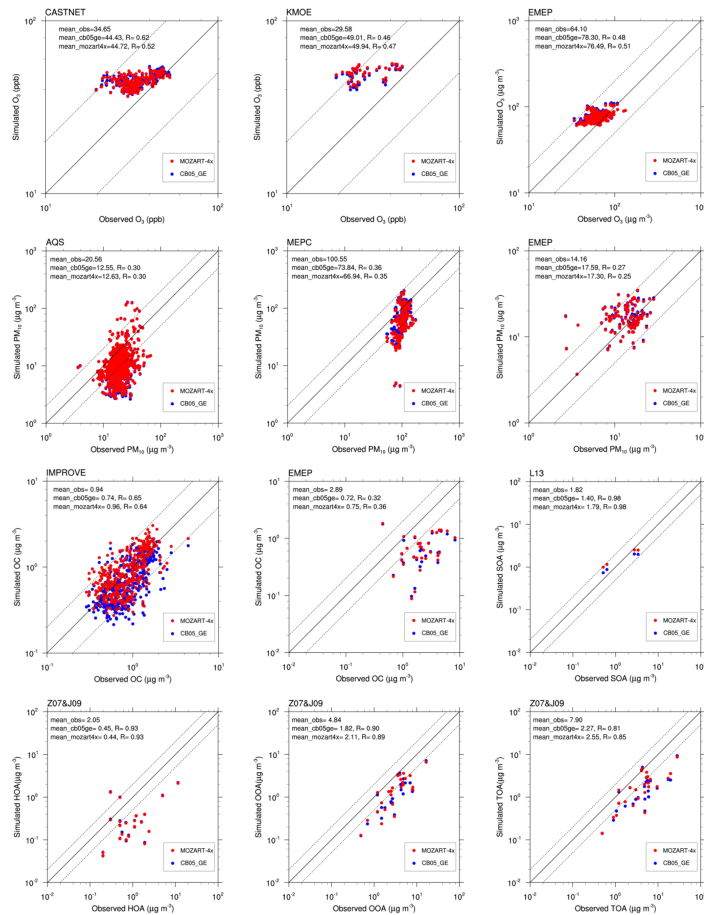
Printer-friendly Version

Interactive Discussion



CESM/CAM5 improvement and application

J. He et al.



[Title Page](#)
[Abstract](#) [Introduction](#)
[Conclusions](#) [References](#)
[Tables](#) [Figures](#)

⏪ ⏩
⏴ ⏵

[Back](#) [Close](#)

[Full Screen / Esc](#)

[Printer-friendly Version](#)
[Interactive Discussion](#)



CESM/CAM5
improvement and
application

J. He et al.

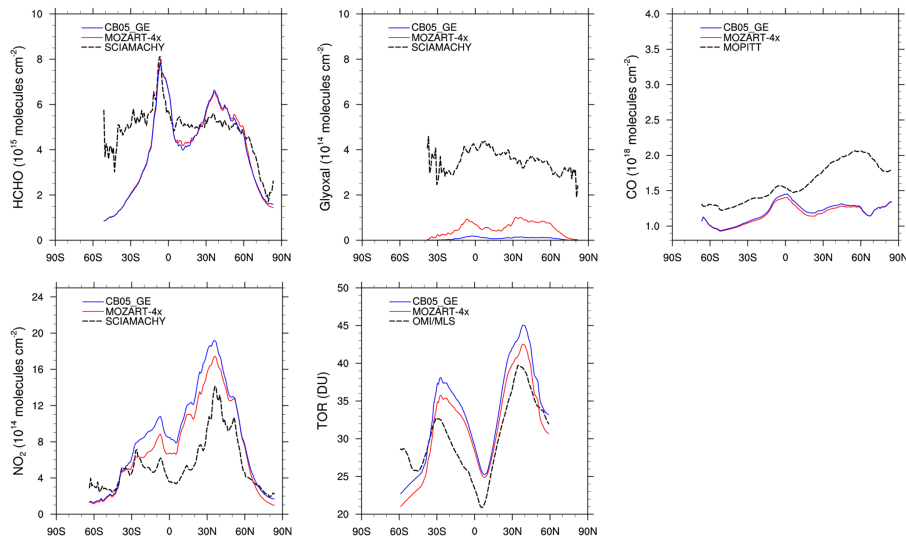


Figure 3. Zonal-mean profiles of HCHO, glyoxal, CO, NO₂, and TOR from CB05_GE and MOZART-4x simulations for June, July, and August during 2008–2010.

Title Page

Abstract

Introduction

Conclusions

References

Tables

Figures



Back

Close

Full Screen / Esc

Printer-friendly Version

Interactive Discussion



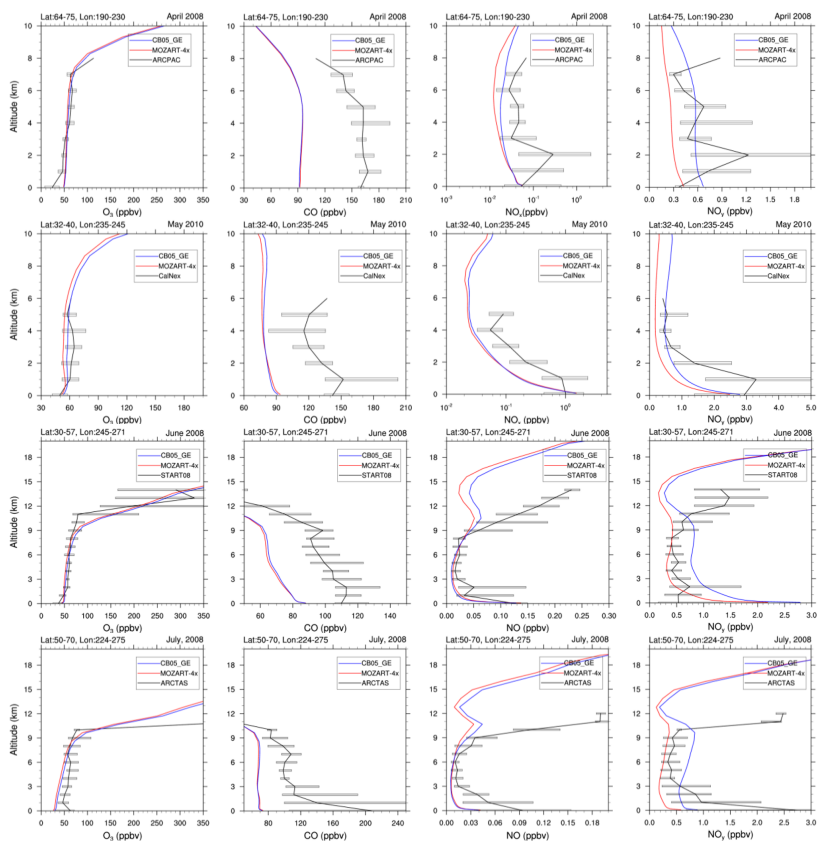


Figure 4. Simulated vertical profiles of O_3 , CO, NO_x , and NO_y , against aircraft measurements. The black solid line represents observations from aircraft measurements (Pan et al., 2010; Brock et al., 2011; Ryerson et al., 2011; Jacob et al., 2010). The red solid and blue solid lines represent model output from MOZART-4x and CB05_GE, respectively.

[Title Page](#)
[Abstract](#)
[Introduction](#)
[Conclusions](#)
[References](#)
[Tables](#)
[Figures](#)

[Back](#)
[Close](#)
[Full Screen / Esc](#)
[Printer-friendly Version](#)
[Interactive Discussion](#)


CESM/CAM5
improvement and
application

J. He et al.

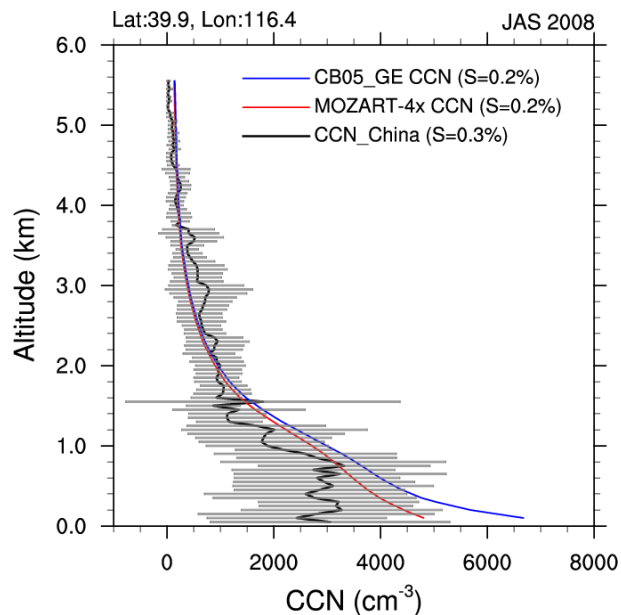


Figure 5. Simulated vertical profiles of CCN against aircraft measurements. The black solid line represents observations from aircraft measurements of Zhang et al. (2011). The red solid and blue solid lines represent model output from MOZART-4x and CB05_GE, respectively.

[Title Page](#)[Abstract](#)[Introduction](#)[Conclusions](#)[References](#)[Tables](#)[Figures](#)[◀](#)[▶](#)[◀](#)[▶](#)[Back](#)[Close](#)[Full Screen / Esc](#)[Printer-friendly Version](#)[Interactive Discussion](#)

CESM/CAM5 improvement and application

J. He et al.

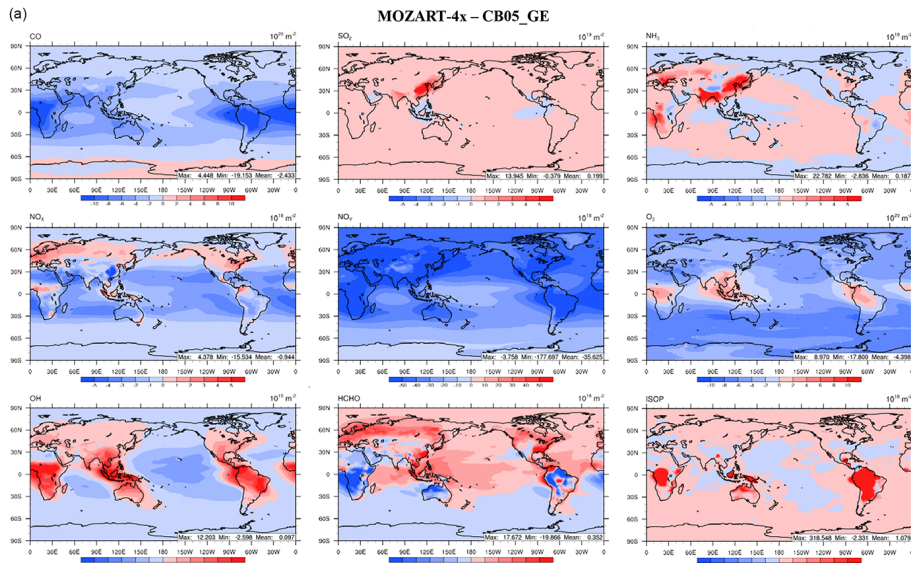


Figure 6.

Title Page

Abstract

Introduction

Conclusions

References

Tables

Figures



Back

Close

Full Screen / Esc

Printer-friendly Version

Interactive Discussion



Title Page

Abstract

Introduction

Conclusions

References

Tables

Figures



Back

Close

Full Screen / Esc

Printer-friendly Version

Interactive Discussion

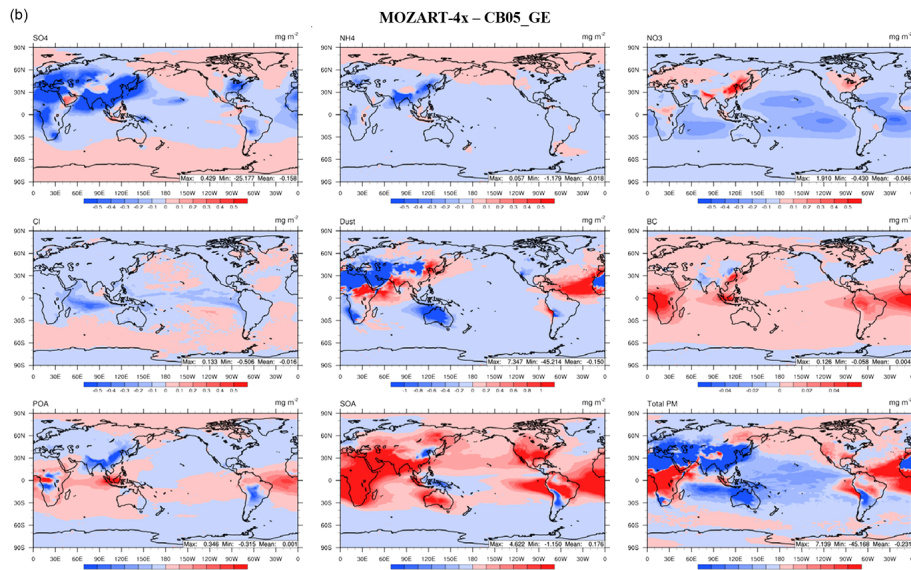


Figure 6. (a) Absolute differences averaged during 2008–2010 in tropospheric column concentrations of major gaseous species between MOZART-4x and CB05_GE. (b) Absolute differences averaged during 2008–2010 in tropospheric column concentrations of major aerosol species between MOZART-4x and CB05_GE.

[Title Page](#)
[Abstract](#)
[Introduction](#)
[Conclusions](#)
[References](#)
[Tables](#)
[Figures](#)

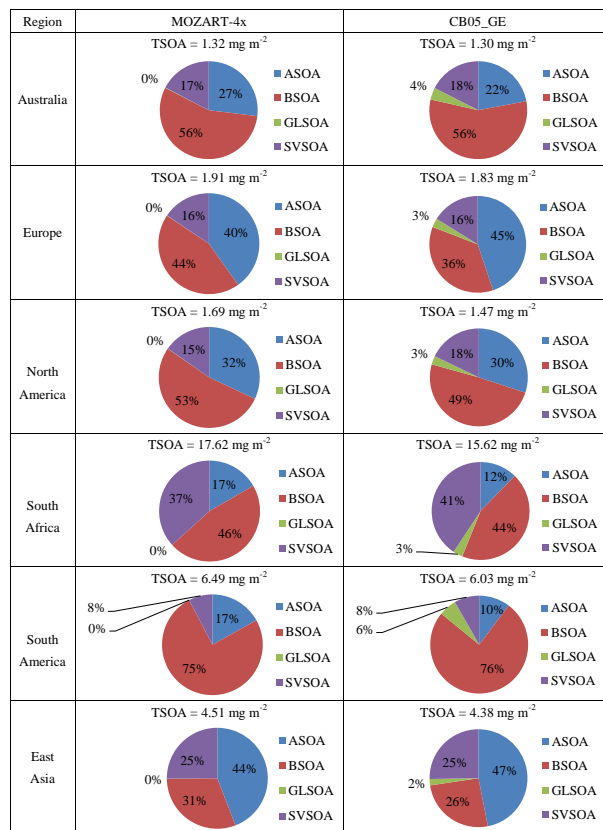
[Back](#)
[Close](#)
[Full Screen / Esc](#)
[Printer-friendly Version](#)
[Interactive Discussion](#)


Figure 7. Column abundances (mg m⁻²) averaged during 2008–2010 of secondary organic aerosols (SOA) from anthropogenic sources (ASOA), biogenic sources (BSOA), and glyoxal (GLSOA), and semi-volatile organic aerosol (SVSOA) over Australia, Europe, North America, South Africa, South America, and East Asia.

CESM/CAM5 improvement and application

J. He et al.

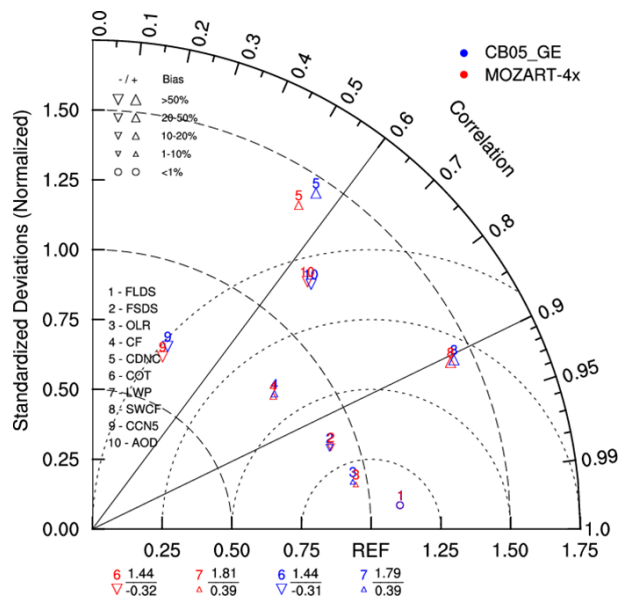


Figure 8. Taylor diagram of comparison of cloud and radiative predictions between MOZART-4x and CB05_GE. The results are based on 3-year average. This diagram represents the similarity between MOZART-4x and CB05_GE. x axis represents the ratio of variances between observations and simulations (proportional to the reference point identified as “REF”), and y axis represents the normalized standard deviation between the two patterns (proportional to the radial distance from the origin). Two variables, COT and LWP, are located outside the diagram because the ratios of variance between simulated results and observations (the values of 1.81 from MOZART-4x and 1.79 from CB05_GE in the top) are larger than 1.75 for LWP and the correlation coefficients (the values of -0.32 from MOZART-4x and -0.31 from CB05_GE in the bottom) for COT are negative.

Title Page

Abstract

Introduction

Conclusions

References

Tables

Figures



Back

Close

Full Screen / Esc

Printer-friendly Version

Interactive Discussion



CESM/CAM5 improvement and application

J. He et al.

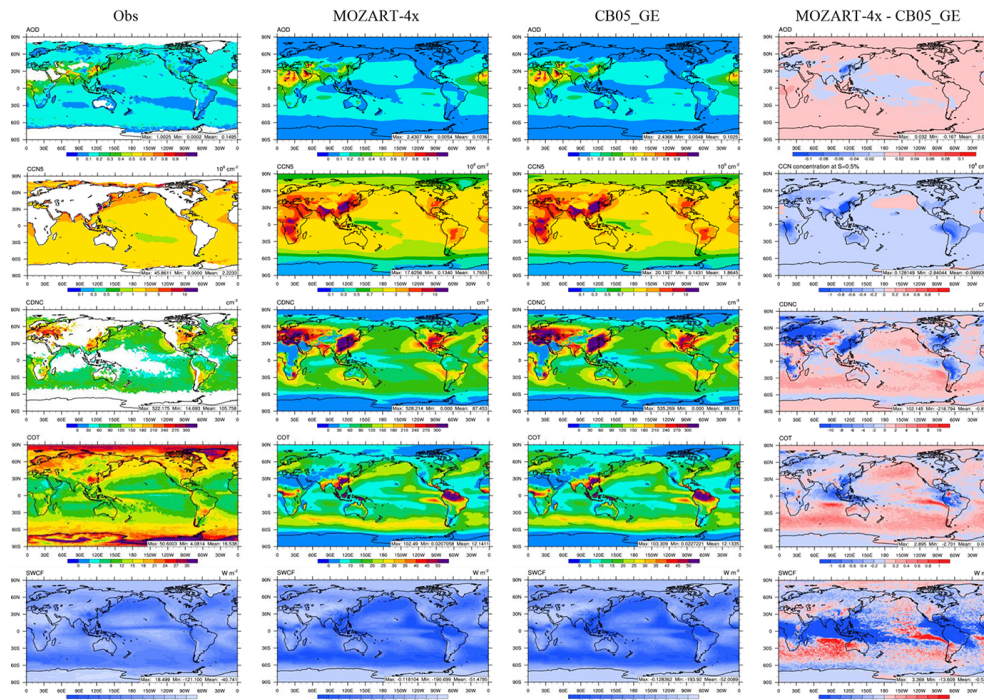


Figure 9. Comparison of satellite observations with predictions of AOD, CCN5, CDNC, COT, and SWCF by MOZART-4x and CB05_GE.

Title Page

Abstract

Introduction

Conclusions

References

Tables

Figures



Back

Close

Full Screen / Esc

Printer-friendly Version

Interactive Discussion

